

Analysis of recent Oceanographic Data for the Mediterranean Sea

October 2020

Faidra Antoniadou

University of Cyprus
Oceanography Center

Abstract

A project to objectively analyze a large quantity of oceanographic data for the Mediterranean sea is described. Preliminary results are encouraging within the limits of data available. Results were used to determine trends in Sea Surface Temperature (SST), Sea Surface Salinity (SSS) and Sea Surface Height (SSH) for the entire Mediterranean as well as for the regions around the estuaries of the rivers Rhone, Evros, Nile and Po. It was calculated that all of SSH, SST and SSS are increasing, on average, with time in all estuary regions as well as the Mediterranean Sea as a whole. Quantitatively, SST has been increasing with $0.0296 \text{ }^{\circ}\text{C yr}^{-1}$, SSS with $0.088 \text{ psu yr}^{-1}$ and SSH with 0.84 mm yr^{-1} since 1987 in the Mediterranean Sea. A brief discussion of the data used, the method of analysis, and some preliminary results are presented.

1 Introduction

The aim of this project is to analyse oceanographic data from the Mediterranean for the period 1987 - 2018 in order to identify patterns in SSS, SST and SSH over time.

1.1 Data and data processing

Data analysis for all parameters mentioned in this paper, including SSS, SST and SSH, has been conducted using E.U. Copernicus Marine Service Information, namely using the product MEDSEA.REANALYSIS_PHYS_006.004. The aim of the MEDSEA.REANALYSIS_PHYS_006.004 is to provide an integrated set of information consistent across space-time dimension, using both observations and model, covering the period 1987-2018. COPERNICUS, previously known as GMES (Global Monitoring for Environment and Security), is the European Programme for the establishment of a European capacity for Earth Observation and Monitoring.

The Mediterranean Forecasting System, physical reanalysis component, is a hydrodynamic model, supplied by the Nucleus for European Modelling of the Ocean (NEMO), with a variational data assimilation scheme (OceanVAR) for temperature and salinity vertical profiles and satellite Sea Level Anomaly along track data. The model horizontal grid resolution is $1/16^{\circ}$ (ca. 6-7 km) and the unevenly spaced vertical levels are 72 [1]. In this paper, only the top level (surface depth at 1.0182 m) is used in the analysis.

The European Space Agency (ESA) is responsible for the space component of the Copernicus programme. The European Organisation for the Exploitation of Meteorological Satellites (EUMETSAT) is fundamental to the operational remit of Copernicus on account of their unparalleled experience and proven capability as a provider of operational meteorological satellite data, products and services.

1.2 Sea Surface Temperature

Sea surface temperature (SST) is the water temperature close to the ocean's surface.

The exact meaning of surface varies according to the measurement method used, but it is between 1 mm and 20 m below the sea surface. [4]

For oceanographers, meteorologists and climatologists, it is one of the signs/results of the exchange of energy between the ocean and the atmosphere. Sea surface temperature varies between -1.8 °C, temperature at which sea water freezes, and +30 °C near/below the Equator [5].

SST is an important variable to better understand interactions between the ocean and the atmosphere. SST analyses convert irregularly spaced SST data to a regular grid and have been used for many purposes from climate monitoring and prediction (e.g., Smith and Reynolds 2003) to feature tracking (e.g., Quartly and Srokosz 2002). Often the planned purpose for the analysis strongly influences the analysis resolution and accuracy.

The ocean model supplied by NEMO, solves the primitive equations in spherical coordinated and has been implemented in the Mediterranean at $1/16^\circ \times 1/16^\circ$ horizontal resolution and 72 unevenly spaced vertical layers (Oddo et al., 2009). The model covers the Mediterranean Basin and also extends into the Atlantic in order to better resolve the exchanges with the Atlantic Ocean at the Strait of Gibraltar. The assimilated data consist of satellite SLA data and in-situ temperature and salinity profiles.

The Mediterranean Sea Physical reanalysis has been initialized by a temperature and salinity monthly climatology (named SDN_V2aa) produced within the framework of SeaDataNet FP6 Project. It was initialized on the 1st of January 1985 and run till the 31st of December 2018.

The evolution of SST error shows a seasonality, with error higher during summer period, during which the system shows a warm bias, and a mean value of 0.56 °C. The SST quality might be considered of comparable quality of satellite optimally interpolated maps (Marullo et al., 2008) [6].

1.3 Sea Surface Height

The sea surface is anything but flat. There are bumps and troughs, all due to different physical characteristics such as gravity, currents, temperature and salinity. Since we do not know much about the ocean's bottom, it is easier to refer to "sea height" instead of sea depth. Sea level is measured with reference to a fixed surface height. By analyzing variations from this reference point, scientists determine ocean circulation (currents and eddies at the edges of holes and bumps), seasonal or inter-annual variations, or even longer periods (long-term rise in sea level).[8]

Satellite altimetry is used to measure sea surface height relative to a reference ellipsoid of the Earth. These height measurements are composed of two components: a time-variant one (due to ocean current variability) and a time-invariant one (due to a combination of spatial variations in the Earth's gravity field and mean ocean dynamic topography). The time-variant component can be separated further into signals of differing temporal and spatial scales. Altimetry has been successfully used to extract information concerning the mesoscale or "eddy-containing" band, defined to encompass spatial scales of between 50 and 500 km, and periods of between 20 and 150 days (McClean et al., 1997), although the upper limit of the spatial scales is extended to 1000 km by some authors (Fu and Cheney, 1995). Generally, the largest errors in the altimeter measurement system are due to poor orbit determination, introducing uncertainties at wavelengths greater than 1000 km. At shorter wavelengths the effect of these errors is reduced. Even the early, relatively crude altimeters such as Geos-3 and Seasat were used to

study mesoscale signals (e.g., Cheney et al., 1983; Fu et al., 1987). Until recently, altimetry has been used with limited success to study the large-scale ocean circulation variability, which generally refers to length scales greater than 1000 km. At these longer wavelengths, errors due to poor orbit determination, tide models, and propagation delay corrections begin to dominate. However, by carefully removing residual orbit error, several authors have been successful in mapping large-scale variability. For example, Chelton et al. (1990) used the Geosat altimeter to map the large-scale variability of the Antarctic Circumpolar current, and Nerem et al. (1994) used TOPEX/Poseidon with its superior orbit accuracy to study large-scale variability of the global ocean.

In addition to the study of ocean variability, satellite altimetry has been applied to the measurement of the time invariant component of sea surface height, or mean sea surface, on a global basis [e.g., Marsh et al., 1992; Marsh and Martin, 1982]. This mean sea surface is composed of two components. First, the geopotential surface (geoid) which is related to the distribution of mass within the Earth, and at shorter wavelengths bathymetry. Second, the mean ocean dynamic topography which is related to the general ocean circulation. The former dominates the vertical deflection by 2 orders of magnitude (100 m versus 1 m), and can therefore be used in lieu of a geoid when a direct estimate of the geoid is not available. Altimetry can also be used to generate gravity fields of the Earth's surface (e.g., the Arctic gravity field of Laxon and McAdoo [1994]) which essentially reveal short wavelength features of the Earth's upper crust. The combination of orbit and geoid error make a determination of the mean ocean dynamic topography very difficult using altimetry. Geographically correlated orbit error, which cannot be reduced by averaging in time, must be reduced by improving gravity models. The accuracy of the TOPEX/Poseidon orbits, and recent improvements in the accuracy of the ERS orbits [Scharroo and Visser, 1998] have made the determination of the dynamic topography a feasible option [e.g., Nerem et al., 1994; Stammer and Wunsch, 1994; Tapley et al., 1994]. Such studies are currently hampered by the fact that the geoid is poorly known at wavelengths of less than about 2500 km [Nerem et al., 1994], resulting in a contamination of the dynamic topography at wavelengths shorter than this. Future satellite missions aimed at improving our knowledge of the Earth's gravity field at shorter wavelengths will permit a more detailed study of the mean dynamic topography (e.g., the NASA Gravity Recovery and Climate Experiment (GRACE) mission [Wahr et al., 1998] and the ESA Gravity Field and Steady state Ocean Circulation Explorer Mission (GOCE) [Rebhan et al., 2000]).[9]

1.4 Salinity

Salinity represents the concentration of dissolved inorganic salts in seawater (grams of salt per kilogram seawater, or parts per 1000, and historically given by the symbol ‰). Oceanographers have developed modern techniques based on the electrical conductivity of seawater, which permit accurate measurement by use of automated electronic in situ sensors. Salinity is derived from conductivity, temperature, and pressure with an international standard set of empirical equations known as the Practical Salinity Scale, established in 1978 (PSS-78) which is much easier to standardize and more precise than previous chemical methods and which numerically represents grams per kilogram. Accordingly, the modern literature often quotes salinity measurements in practical salinity units (psu) or refers to PSS-78 [17].

In 1982, the need to re-evaluate the salinity scale led the Joint Panel to recommend (jspots, 1981; Lewis, 1980)

that salinity be defined using only conductivity, breaking the link with chlorinity. All water samples with the same conductivity ratio have the same salinity even though their chlorinity may differ. The PSS-78 defines Salinity as:

$$S = 0.0080 - 0.1692K_{15}^{1/2} + 25.3851K_{15} + 14.0941K_{15}^{3/2}7.0261K_{15}^2 + 2.7081K_{15}^{5/2}$$

$$K_{15} = C(S, 15, 0)/C(KCl, 15, 0)$$

$$2 \leq S \leq 42$$

where $C(S, 15, 0)$ is the conductivity of the sea-water sample at a temperature of 14.996°C on the International Temperature Scale of 1990 and standard atmospheric pressure of 101 325 Pa, having a salinity S derived as above. $C(KCl, 15, 0)$ is the conductivity of the standard potassium chloride (KCl) solution at a temperature of 15°C and standard atmospheric pressure. The standard KCl solution contains a mass of 32.4356 grams of KCl in a mass of 1.000 000 kg of solution.

The Practical Salinity Scale of 1978 introduced several small problems. It led to confusion about units and to the use of “practical salinity units” that are not part of the definition of Practical Salinity. In addition, absolute salinity differs from salinity by about 0.5%. And the composition of seawater differs slightly from place to place in the ocean, leading to small errors in measuring salinity. To avoid these and other problems, Millero et al (2008) defined a new measure of salinity, the Reference Salinity, that accurately represents the Absolute Salinity of an artificial seawater solution. It is based on a Reference Composition of seawater. The Reference Composition of the artificial seawater is defined by a list of solutes and their mole fractions given in Table 4 of their paper. From this, they defined artificial Reference Seawater to be seawater having a Reference Composition solute dissolved in pure water as the solvent, and adjusted to its thermodynamic equilibrium state. Finally, the Reference Salinity of Reference Seawater was defined to be exactly $35.16504 \text{ g kg}^{-1}$. With these definitions, plus many details described in their paper, Millero et al (2008) show Reference Salinity (S_R) is related to Practical Salinity by:

$$S_R \approx (35.16504/35)\text{gkg}^{-1} \times S$$

The equation is exact at $S = 35$. S_R is approximately 0.47% larger than Practical Salinity. Reference Salinity S_R is intended to be used as an SI-based extension of Practical Salinity [18].

Salinity ranges from near zero adjacent to the mouths of major rivers to more than 40 in the Red Sea. Aside from such extremes, open ocean surface values away from coastlines generally fall between 32 and 37 [17]. It is not fixed by any equilibria, feedbacks, or geochemical cycles and appears to have been generally higher in past times. It is apparently a free variable dependent upon the vagaries of intermittent salt (and brine) sequestration on long-lived continental cratons. Ocean salinity declines when the salt and brine accumulate and rises when they are eroded back into the sea. [7]

Salinity is an important measurement in seawater or in estuaries where freshwater from rivers and streams mixes with salty ocean water. The salinity level in seawater is fairly constant, at about 35 ppt (35 000 mg/L), while

brackish estuaries may have salinity levels between 1 and 10 ppt. Since most anions in seawater or brackish water are chloride ions, salinity can be determined from chloride concentration. A Chloride Ion-Selective Electrode can be used to determine the chloride concentration, which is converted to a salinity value.

1.5 Geographic Regions Analysed

For the purposes of this project, data for specific regions in the Mediterranean Sea have been analysed; the analysis was carried out for the entire Mediterranean, subsequently focusing on regions close to river estuaries. The rivers we will focus on are the Nile, Evros, Rhone and Po as they are amongst the rivers with the highest annual climatological river discharge and in different regions of the Mediterranean Sea.

The Mediterranean Sea is an intercontinental sea that stretches from the Atlantic Ocean on the west to Asia on the east and separates Europe from Africa. The western extremity of the Mediterranean Sea connects with the Atlantic Ocean by the narrow and shallow channel of the Strait of Gibraltar, which is roughly 8 miles (13 km) wide at its narrowest point; and the depth of the sill, or submarine ridge separating the Atlantic from the Alborán Sea, is about 1 050 feet (320 m). To the northeast the Mediterranean is connected with the Black Sea through the Dardanelles (with a sill depth of 70 m), the Sea of Marmara, and the strait of the Bosphorus (sill depth of about 90 m). To the southeast it is connected with the Red Sea by the Suez Canal.[10]

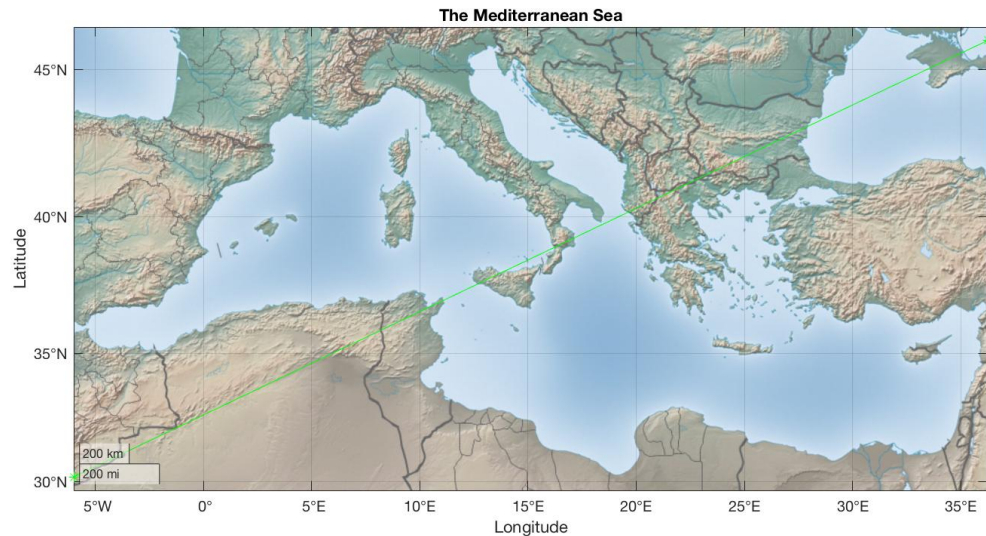


Figure 1: Map of the Mediterranean Sea region used in subsequent analysis. The sections of the Atlantic Ocean as well as the Black Sea which appear in the map were excluded from the analysis.

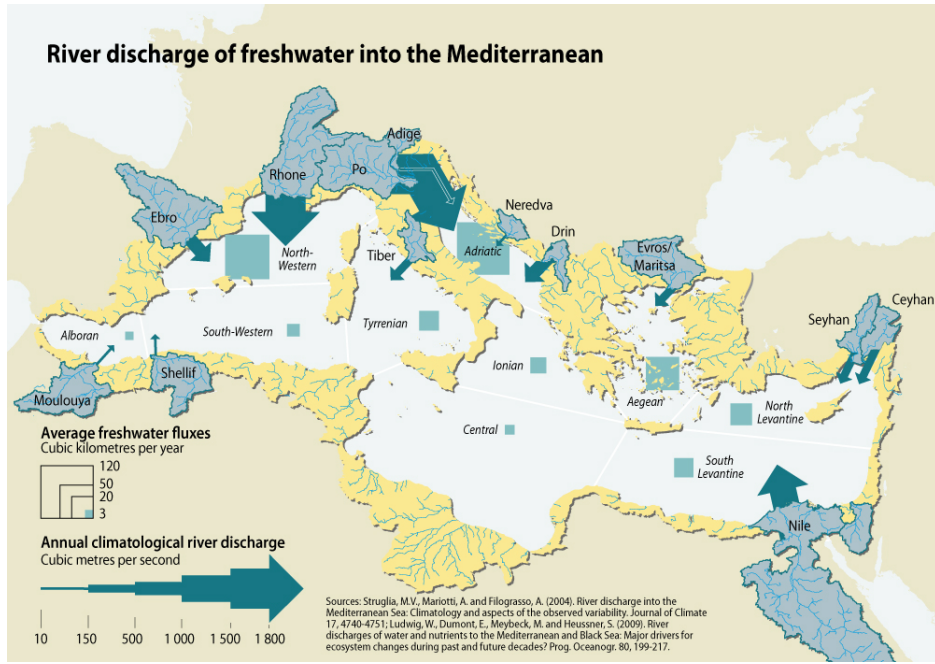


Figure 2: Major river discharge of freshwater areas in the Mediterranean Sea; some of the most largest annual climatological river discharge in volume originate from the rivers Po, Rhone and Nile.

Source: 2013.GRID-Arendal [Online]. Available: <https://www.grida.no/resources/5897>

The Nile River is one of the largest rivers of the world and its spatial division of water supply and demand is high. The majority of supply is accounted for by rainfall upstream in the Blue and White Nile tributaries, demands are highest downstream, in Sudan and Egypt [11]. It rises south of the Equator and flows northward through northeastern Africa to drain into the Mediterranean Sea. It has a length of about 4 132 miles (6 650 kilometres) and drains an area estimated at 1 293 000 miles² (3 349 000 km²). The Nile delta comprises a gulf of the prehistoric Mediterranean Sea that has been filled in; it is composed of silt brought mainly from the Ethiopian Plateau. The silt varies in its thickness from 50 to 75 feet and comprises the most fertile soil in Africa. It forms a monotonous plain that extends 100 miles from north to south, its greatest east–west extent being 155 miles between Alexandria and Port Said; altogether it covers an area twice that of the Nile valley in Upper Egypt [12].

The Evros River, also called Marica, Greek Évros, Turkish Meriç, is a river in Bulgaria, rising in the Rila Mountains southeast of Sofia on the north face of Musala Peak. It flows east and southeast across Bulgaria for 170 miles (275 km), forms the Bulgaria–Greece frontier for a distance of 10 miles (16 km), and then becomes the Greece–Turkey frontier for another 115 miles (185 km). At Edirne it changes direction, flowing south and then southwest to enter the Aegean Sea. Major tributaries are the Arda, Stryama, Topolnitsa, and Tundzha. The area of its drainage basin is 20 000 miles² (53 000 km²). [13]

Rhône (Rhone) River, is a historic river of Switzerland and France and one of the most significant waterways of Europe. It is the biggest European river which flows into the Mediterranean Sea [27] and is thoroughly Alpine in character. In this respect, it differs markedly from its northern neighbour, the Rhine, which leaves all of its Alpine characteristics behind when it leaves Switzerland. The scenic and often wild course of the Rhône, the characteristics

of the water flowing in it, and the way it has been used by humans have all been shaped by the influences of the mountains, right down to the river mouth, where sediments marking the Rhône's birth in an Alpine glacier are carried into the warmer waters of the Mediterranean. The Rhône is 505 miles (813 km) long and has a drainage basin of some 37 750 square miles (97 775 km²). The course of the river can be divided into three sectors, lying respectively in the Alps, between the Alps and the Jura Mountains and through the latter, and finally in the topographical furrow of Alpine origin running from the city of Lyon to the sea. The river's delta begins near Arles and extends about 25 miles (40 km) to the sea. Twin channels of the river, the Grand and Petit Rhône, enclose the Camargue region. This region, formed by alluvium, is continuously extending into the Mediterranean [14].

Po River is known to the public as the longest river entirely flowing in the Italian peninsula, being its main stream about 652 km long [15], rising in the Monte Viso group of the Cottian Alps on Italy's western frontier and emptying into the Adriatic Sea in the east after a course of 405 miles (652 km). Its drainage basin covers 27 062 miles² (70 091 km²), forming Italy's widest and most fertile plain. Its delta is among the most complex of any European river, with at least 14 mouths, usually arranged in five groups (from north to south): the Po di Levante, Po di Maestra, Po della Pila, Po delle Tolle, and Po di Goro e di Gnocca. Of these mouths, the Po della Pila carries the greatest volume of water and is the only navigable one [16].

In the analysis, the regions around the estuaries of the abovementioned rivers, as shown in Table 1, were used. It should be clarified that for the Mediterranean Sea analysis, the Black Sea and the Atlantic Ocean segments included in the geographical coverage were ignored in subsequent analysis.

Region	Geographical Coverage
Mediterranean Sea	6.0000°W - 36.2900°E; 30.1875°N – 45.9375°N
Nile estuary	30.1875°E - 33.3125°E; 30.7500°N - 32.1250°S
Evros estuary	22.0625°E - 28.3125°E; 37.6250°N - 41.3750°N
Po estuary	12.0625°E - 13.8125°E; 43.2500°N - 45.9375°N
Rhone estuary	0.8125°E - 8.3125°E; 42.6250°N - 44.5000°N

Table 1: Table of geographic coordinates of regions analysed in this paper

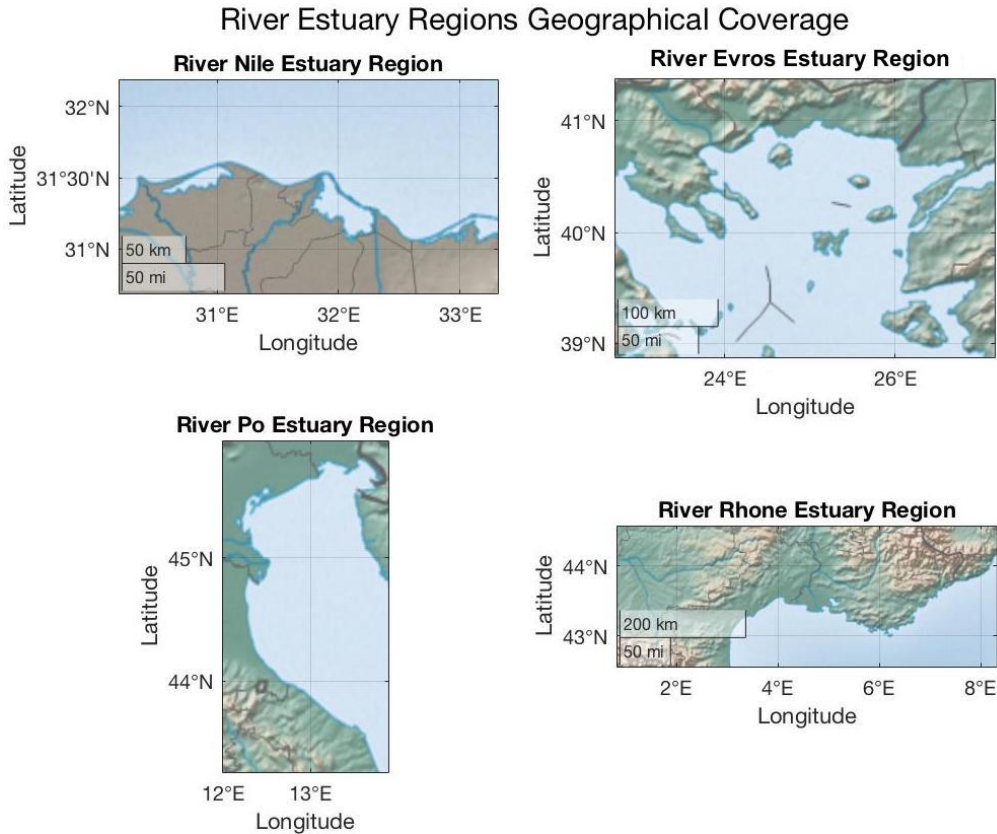


Figure 3: Maps of the estuary regions of the rivers Nile, Po, Maritsa and Rhone. The maps indicate the regions, in terms of latitude and longitude, that have been used in the subsequent analysis.

2 Results & Analysis

In order to carry out data analysis for the parameters mentioned in the introduction section of this paper, MATLAB was used. Data files were downloaded in NetCDF format. The files contain monthly mean averages for each of the parameters at each data point.

In this section the trends that have been observed for salinity, sea surface temperature and height and how these have varied throughout the period between 1987 and 2018, are discussed. Annual Mean Averages were calculated through averaging Monthly Mean Averages as well.

2.1 Trends in the Mediterranean Sea

Sea surface temperature (SST) was analysed for the entire Mediterranean Sea, and maps were produced using the Peak Colour (pcolor) function which linearly maps the elements of the matrix containing all data points in the NetCDF file, to an index into the current colourmap.

There were significant differences between certain months of some years between 1987 and 2018 as in Figure 4.

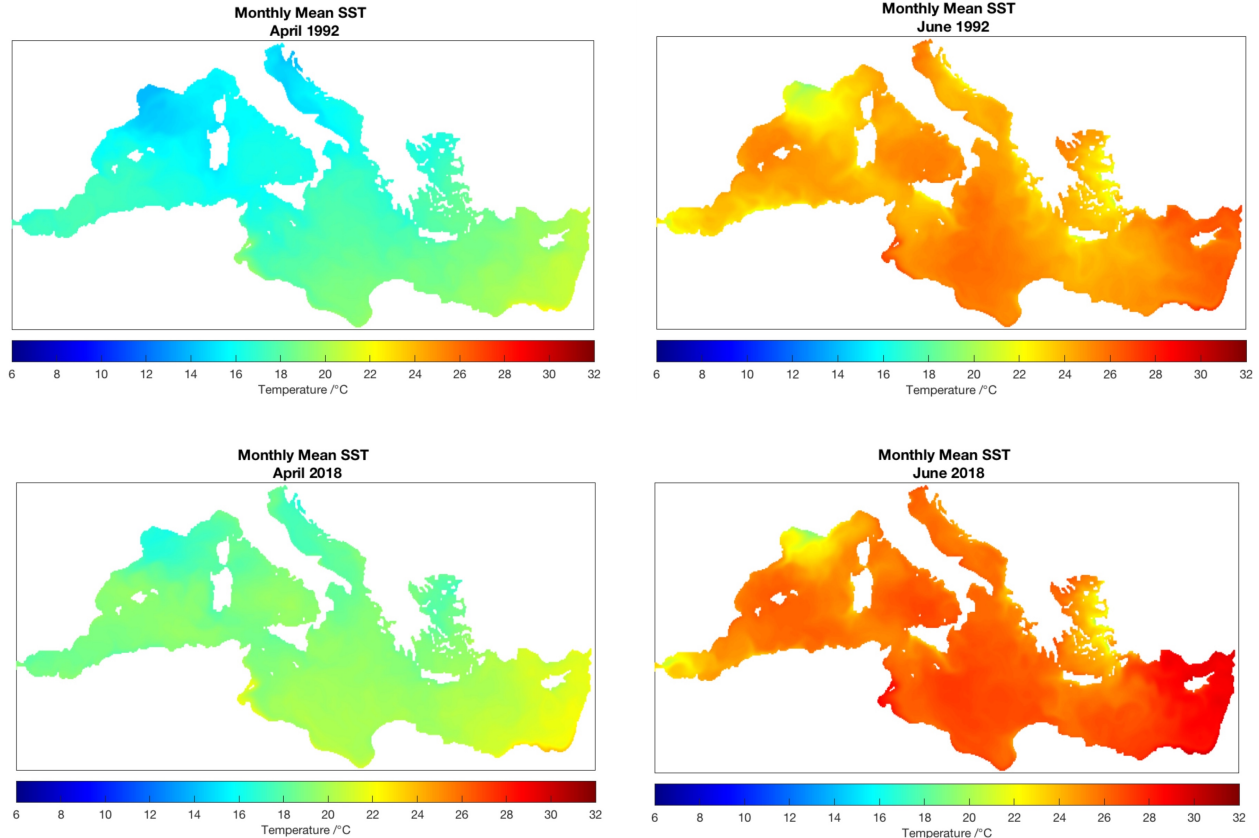


Figure 4: An example of a visibly significant difference of SST in April and June between 1992 and 2018 for the Mediterranean Sea.

In Figure 4 it is clear that SSTs in all regions of the Mediterranean Sea have increased between the two years. For instance, the Levantine Sea seems to have been the warmest area in the Mediterranean Sea with average SSTs of around 19 °C in April 1992 and 25 °C in June, while in 2018 SST rose by around 3 °C. The same holds for the Gulf of Gabès. On the other hand, the Gulf of Lion seems to be one of the coldest areas in the Mediterranean Sea, yet SST increased from 15 °C in April and 21 °C in June 1992, to 17 °C and 23 °C respectively, thus noting an increase of 2 °C with time.

To determine whether the trend for the entire period showed increase of SST with time, mean SST was subsequently calculated for each year, as shown in Figure 5. As the trend showed an approximately linear increase with time, a best-fit straight line was plotted, which allowed for the rate of increase of SST to be calculated.

Though there is an evident increase in SST overall, there are some extreme values in the data, including the year 2003 for which mean SST is 20.45°C - almost as high as 2018 when mean SST rose to 20.48°C, while the year after, a large drop is noted. In addition, one can observe a significant decrease in 1992 when mean SST was calculated to be 19.34 °C.

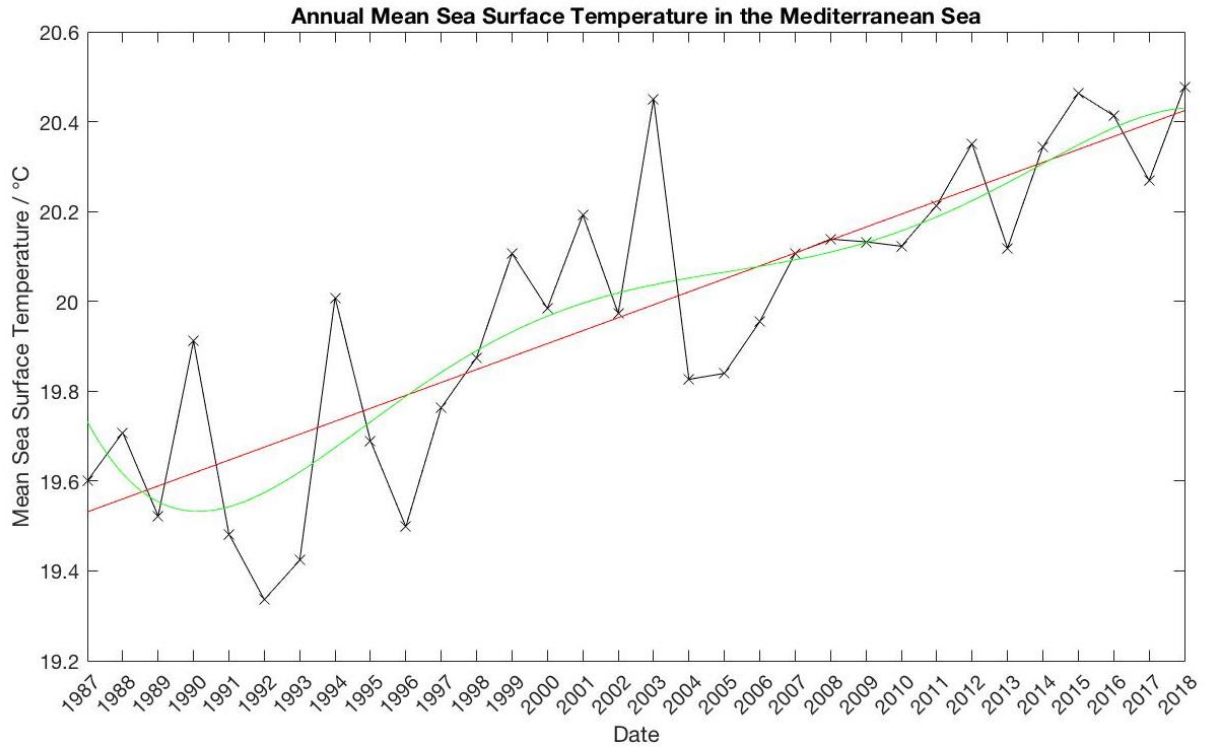


Figure 5: Mean values for the annual mean SST in the Mediterranean Sea plotted against time. The red line portrays a linear increase in SST with time, while the green curve illustrates a non-linear increase.

As shown on Figure 5, SST is increasing with time, despite extreme values. The gradient of the best-fit straight line (i.e., the rate of increase of SST in the Mediterranean Sea) has been calculated to be $0.297 \text{ } ^\circ\text{C year}^{-1}$.

Salinity was also analysed with the same manner, yielding results similar to sea surface temperature. As with SST there is a visible difference between specific months of different years, as shown in Figure 6.

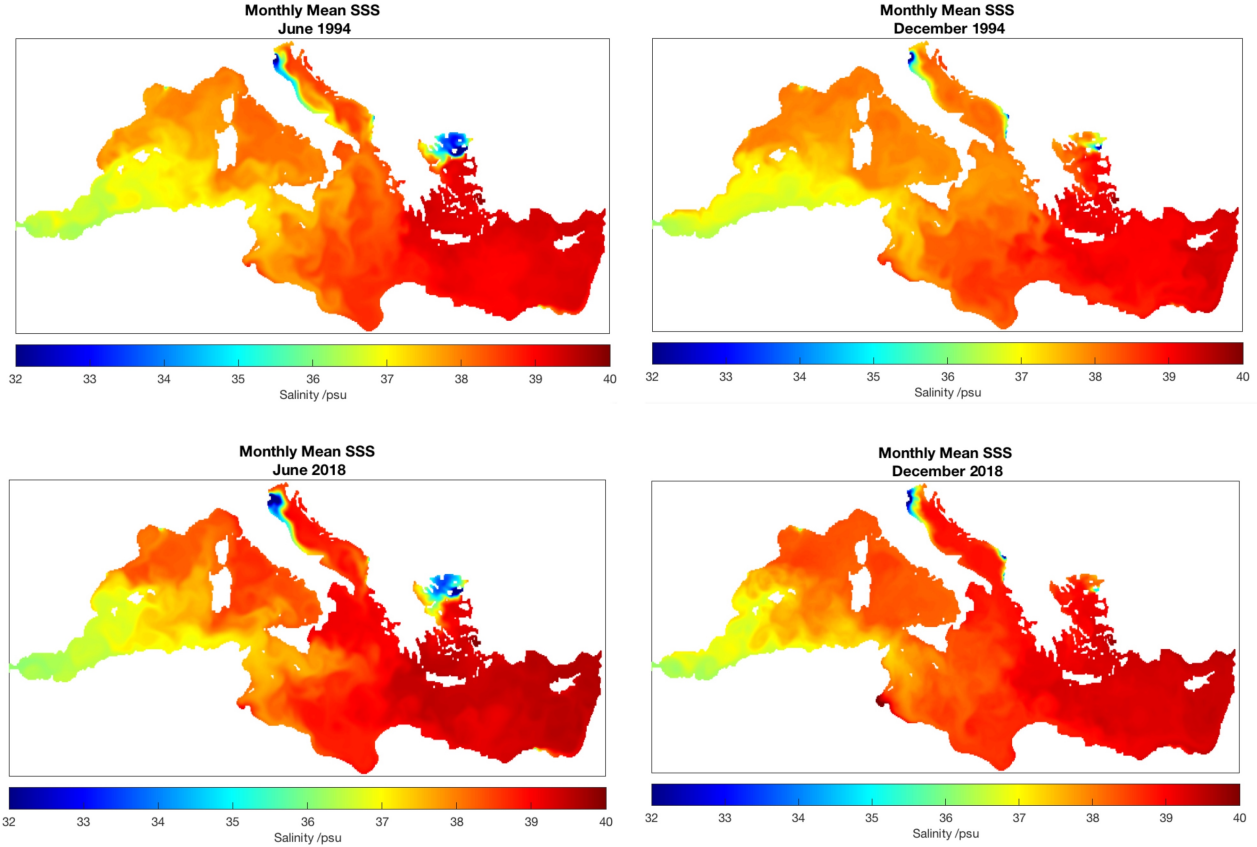


Figure 6: An example of a visibly significant difference in SS in December and June between 1994 and 2018 for the Mediterranean Sea.

As with SST, we note that SSS seems to have increased over the years. In December 1994, SSS in the Adriatic Sea for example, averaged at around 37.5 psu, while in December 2018 it averaged at 38.5 psu; an increase of 1 psu. In June 1994, mean SSS was around 37 psu while in 2018 it increased to 38 psu. This is an increase of 1 psu over that time period. It should be noted that the area with highest SSS throughout appears to be the Levantine Sea as well as some areas in the Aegean Sea, while the one with the lowest SSS is the Alboran Sea where water from the Atlantic enters the Mediterranean Sea through the Strait of Gibraltar. The minimum SSS point values in river estuaries, occur where river streams of freshwater flow in sea saltwater.

In order to determine the trend in the whole Mediterranean Sea with time, as far as SSS is concerned, a graph of Annual Mean SSS was plotted against time, which is shown in Figure 7. To calculate the annual mean, monthly mean values were used. The data showed that SSS has been steadily increasing since 1987 and so a best-fit straight line was plotted using the Polynomial Curve Fitting (polyfit) function in MATLAB as with SST. The gradient of this line was calculated and hence it was determined that the rate of increase of SSS is on average $0.088 \text{ psu yr}^{-1}$. Some extreme values include the years 1997, 2004 which exhibited a much lower value for the annual mean SSS considering the trend. On the other hand, in 1987 annual mean SSS was much higher and a decrease was noted in the following years.

The red best-fit straight line on the graph illustrates that mean SSS in the Mediterranean Sea increases linearly with time. The green best-fit curve (drawn using the polyval and polyfit functions for a fifth-degree polynomial) shows a non-linear increase in SSS with time. An overall increase persists in both cases.

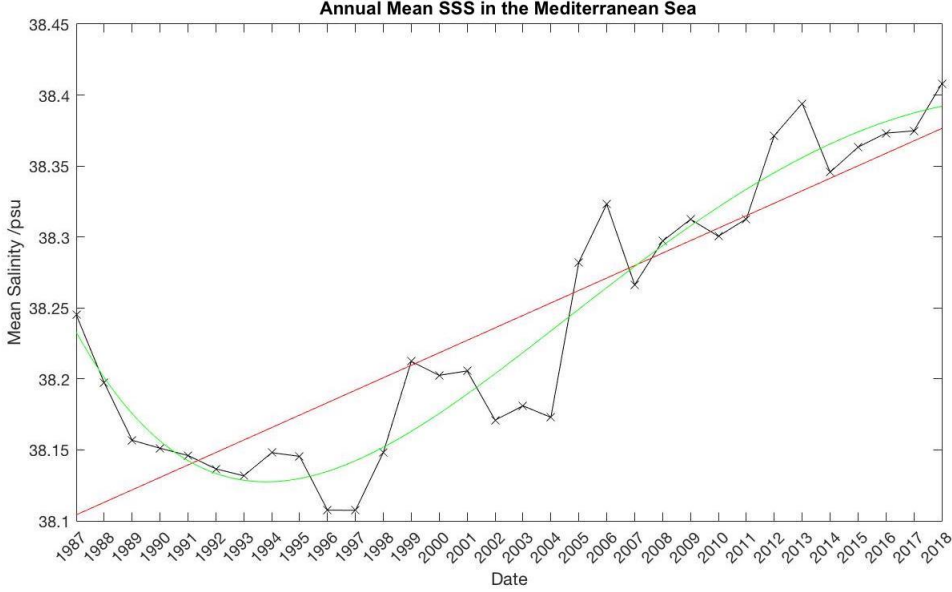


Figure 7: Annual Mean SSS in the whole of the Mediterranean Sea. The trend shows increasing SSSs with time; the red line represents a linear increase in SSS time, while the green curve accounts for fluctuations, portraying a non-linear, increasing trend.

Sea Surface Height (SSH) was analysed as well and through similar analysis, it was determined that there is an evident increase with time as indicated in Figure 8. Although SSS exhibited a decreasing trend between 1987-1997, it began increasing in 1998, consistently increasing, on average, until 2018. The mean rate of increase of SSS was calculated to be $0.0090 \text{ psu yr}^{-1}$.

SSH be expressed in terms of its position with respect to the geoid (SSH above the geoid). The negative values (as in Figure 8) mean it is lower than the geoid, whereas a positive value will mean it is higher than the geoid [28].

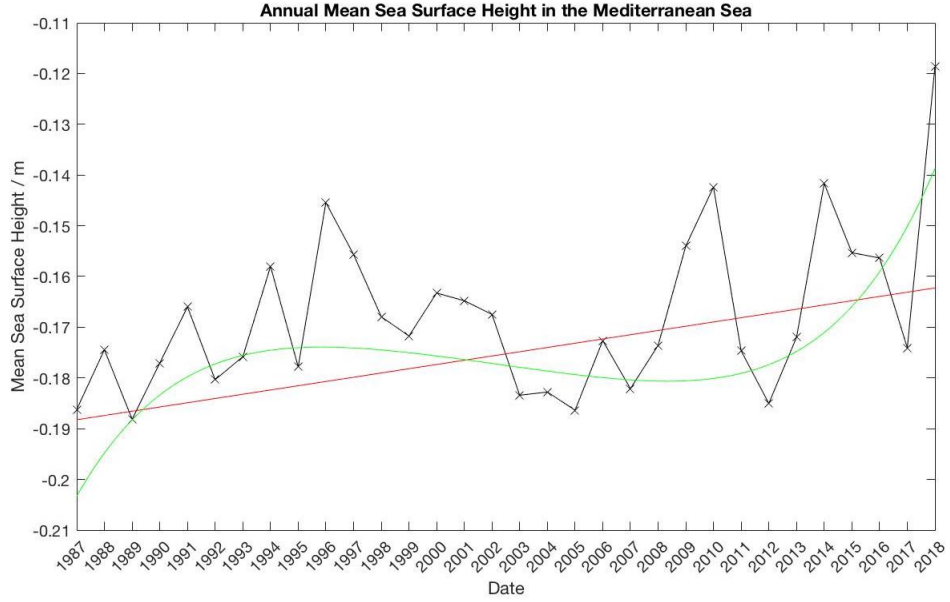


Figure 8: Annual Mean SSH in the Mediterranean Sea plotted against time. On average, SSH has been increasing and the red line examines the case of linear increase with time, while the green curve takes into account fluctuations (particularly a decline in SSH between 1995 and 2009), as well as a sharp increase in 2018. The green line is a third-degree polynomial.

As with SSS and SST, an overall increase in SSH can be observed, with time, in the whole of the Mediterranean Sea. Visible differences between April and November of 1995 and 2015 are illustrated in Figure 9.

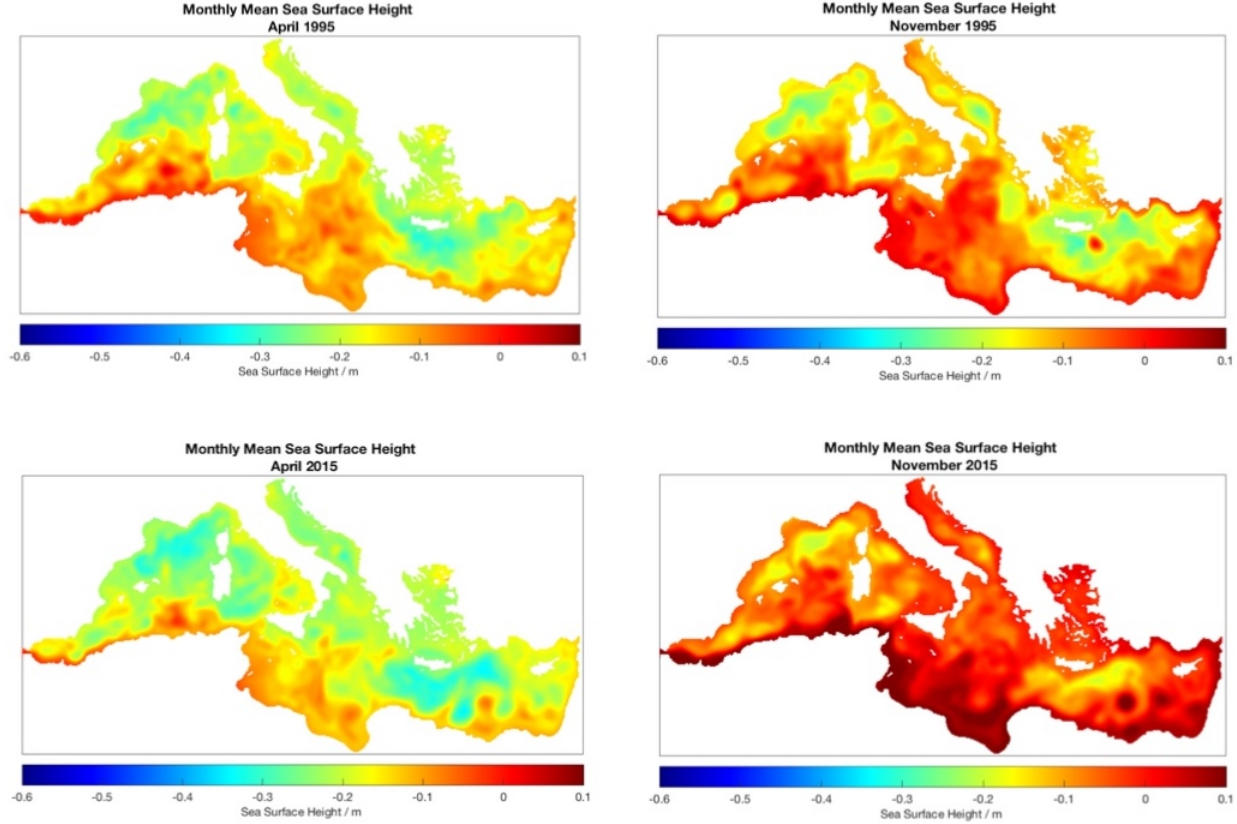


Figure 9: A visual representation of the significant difference in SSH in April and November between 1995 and 2015 for the Mediterranean Sea.

When comparing the gradient of the best-fit straight line of the graph for the annual mean SSH, to those for SSS and SST, one can observe that it demonstrates a much smoother increase. We note some extreme values including the years 2005 and 2012 when SSH was lower than the trend, and 1996 when it was higher. In 2018, SSH increased sharply, increasing from -0.1741 m to -0.1186 m ; a difference of 0.0555 m , making mean SSH in 2018 an extreme value. If 2018 was not taken into account, SSH would have remained virtually constant throughout the time period. Overall, the trend displays that on average, there is an increase of 0.84 mm yr^{-1} . SSH has risen by 6.76 cm since 1987 according to the data.

We also consider accelerating sea level rise since 2005, in which case, Figure 10 indicates that SSH has been rising by 3.8 mm year^{-1} , which is more than four times the rate of increase compared to the time period since 1987.

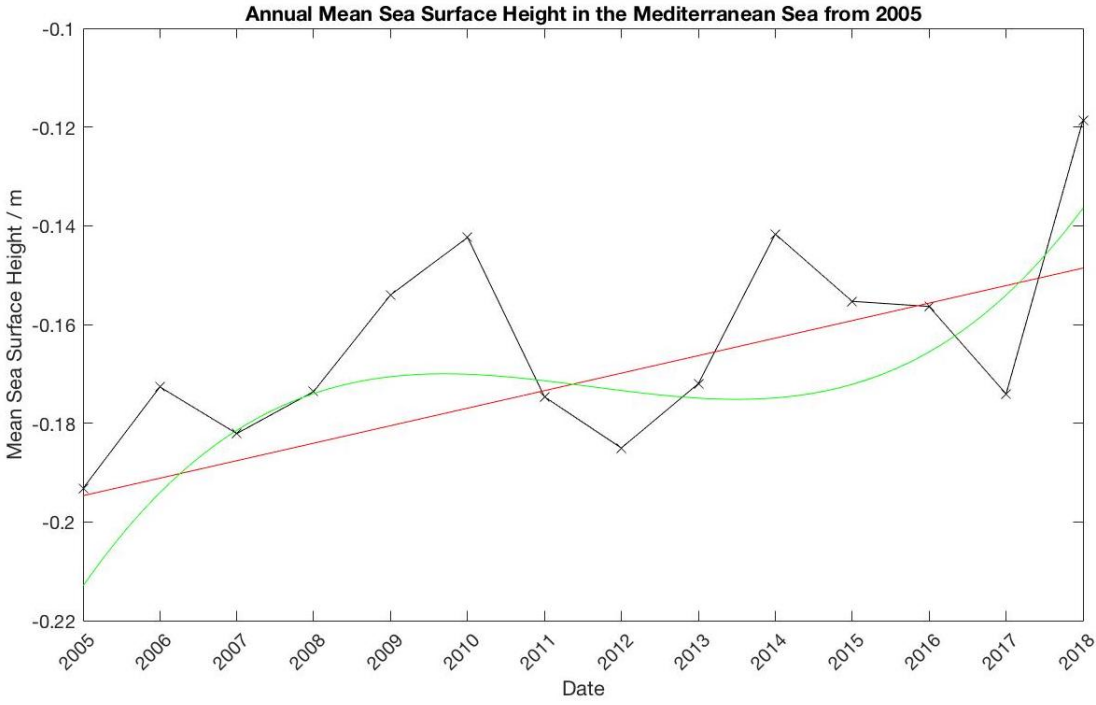


Figure 10: A diagram of Annual Mean SSH against time, exploring the behaviour of SSH in the period 2005-2018 when a sharper increase seems to have been evident. The best-fit green line is a third-degree polynomial.

2.2 Trends in SSS around river estuaries

In this section we will focus on certain areas of the Mediterranean Sea and analyse results for the same parameters, in order to determine how SSH, SST and SSS have been changing in regions of river estuaries. As mentioned previously, analysis has been carried out for the rivers Evros, Po, Rhone and Nile. It should be noted that the geographical coverage of the regions analysed is as listed in Table 1.

To gain an understanding of how conditions change throughout the year in these regions, monthly averages were taken for the years 1988, 1998, 2008 and 2018 for the rivers Nile, Po, Rhone and Evros. The assumption that these conditions exhibit similar trends during a year was made. By taking averages for four different years, we verify that conditions are indeed similar in any year. Excluding extreme weather phenomena and natural disasters, weather conditions during seasons have remained visually constant throughout the years. Figures 11-15, demonstrate changes in SSS.

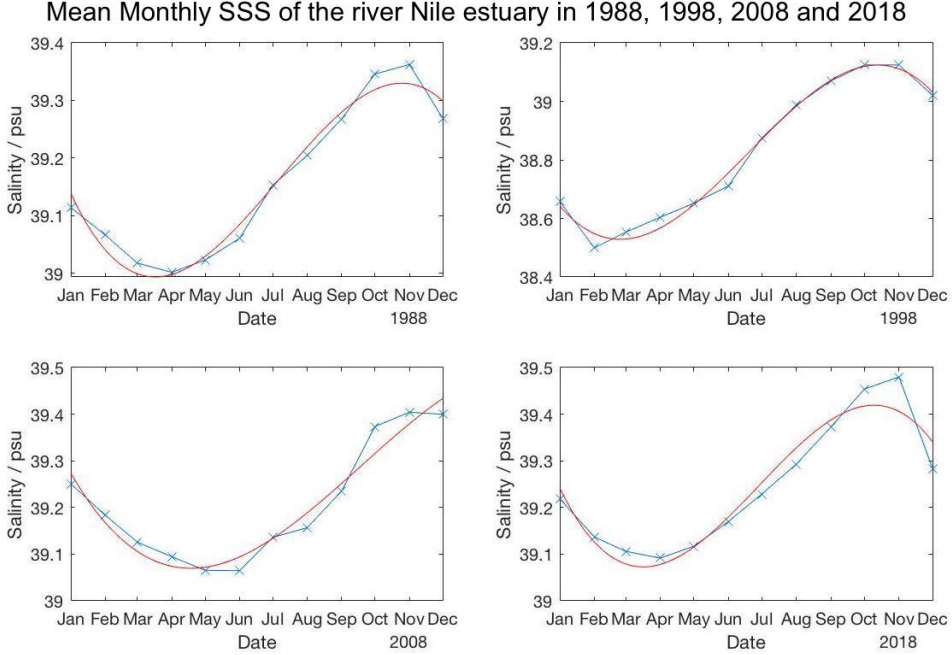


Figure 11: Seasonal changes in SSS for the Nile estuary region; SSS is highest during Autumn and lowest during the spring. The trend fits a third degree polynomial curve.

Figure 11 indicates that SSS in the region of the Nile estuary, is at its highest around October, whereas lowest salinities are observed around March. The best-fit curve shows that SSS decreases between January and March, afterwards increasing steadily until October when it reaches a maximum, subsequently decreasing for the rest of the year. The trend seems to be consistent throughout the years, with no major differences being noted between the four decades. However, Monthly Mean SSS values seem to have increased for each month over the years. In 1988 they were slightly higher than in 1998, though in the two following decades they seem to have increased considerably.

As one can observe in Figure 12, there seems to be a different pattern for the river Evros, with the smallest salinity values being noted mostly around July and maximum salinity during February and March. In January, salinity in the region decreases at an increasing rate, eventually reaching a minimum between July. It then proliferates, reaching another - slightly smaller than February - maximum in December. As with the Nile, salinity over the years seems to have increased over the years.

Mean Monthly SSS of the river Evros estuary in 1988, 1998, 2008 and 2018

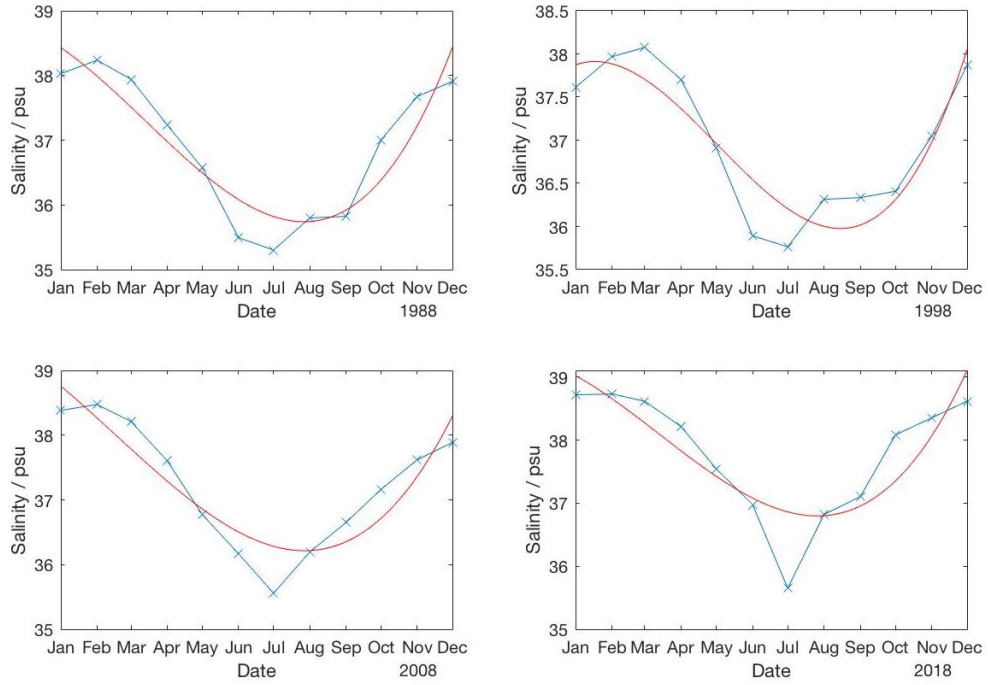


Figure 12: Mean Monthly SSS in the Evros estuary region drops in SSS during spring, with lowest values occurring in June - July - and September in 1988.

Monthly Mean SSS in the region of the river Po estuary exhibits a similar pattern as with Evros, as indicated in Figure 13, with the only difference being that salinity is highest between September and November. In 1988 minimum Monthly Mean SSS lasted from June until September, while in the following decades it was only observed in a single month. Monthly Mean SSS values for each month seem to have increased as with other rivers, though by a larger amount compared to the Nile and Evros. Measurements of Monthly Mean SSS seem to also deviate more from the best-fit curve compared to the Nile.

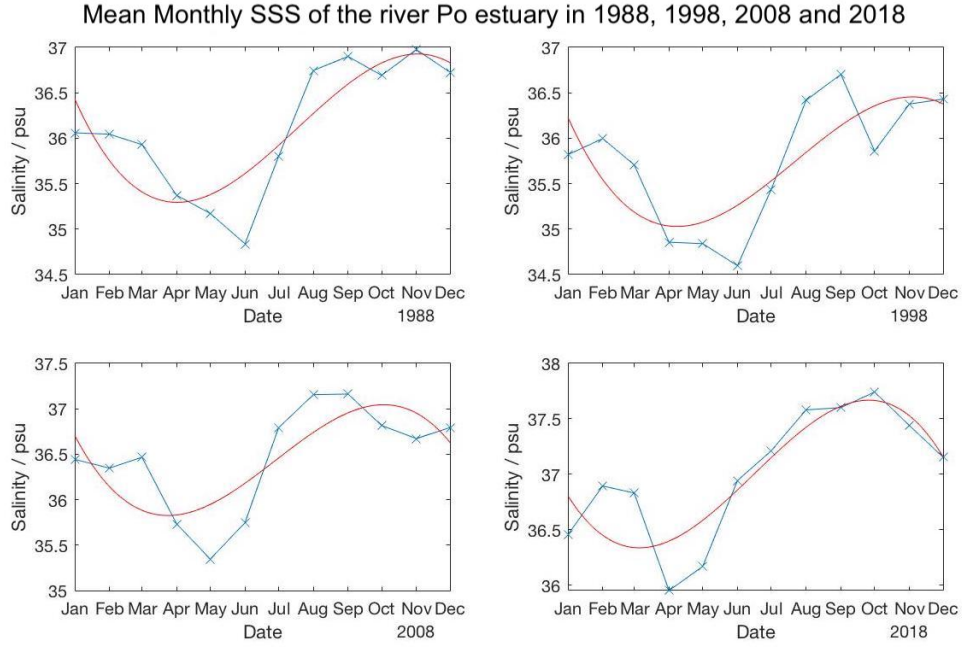


Figure 13: Mean Monthly SSS in the Po estuary region indicates a drop in SSS during spring, with lowest values occurring in May and June.

The region around the estuary of the Rhone has a more diverse pattern from year to year as seen in Figure 14, though minimum values are consistently noted between April and June. Maximum Monthly Mean SSS can be observed either between January and March, or between August and October. Right before and after the month when minimum Monthly Mean SSS occurs, the decrease and increase, respectively, in salinity is rapid. The graphs in Figure 14 show that measurements in this region deviate the most from the best-fit straight line compared to the other regions.

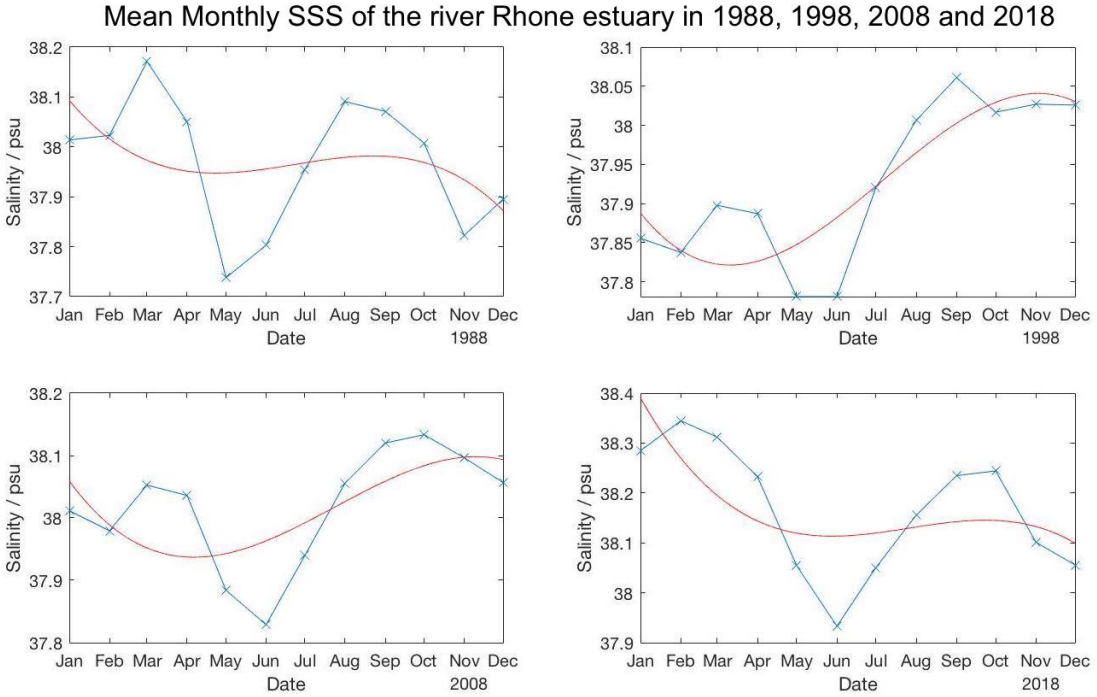


Figure 14: Mean Monthly SSS in the Rhone estuary region indicates a drop in SSS during spring, with lowest values occurring in May and June. Time of occurrence of highest values is inconsistent; it varies between either February and March or September and October. The best-fit curve is inconsistent with the trend.

In Figure 15, we conclude by looking at Monthly Mean SSS values during the same time period for the above river estuary regions. In the Mediterranean Sea minimum Monthly Mean SSS is usually observed around May and June, while maximum Monthly Mean SSS values are noted mostly in September. Overall, the pattern resembles that of rivers Rhone and Po. Salinity has also increased in the Mediterranean Sea throughout the years, fact that is also verified through Figure 7, which shows an increase in the annual mean salinity of the Mediterranean Sea.

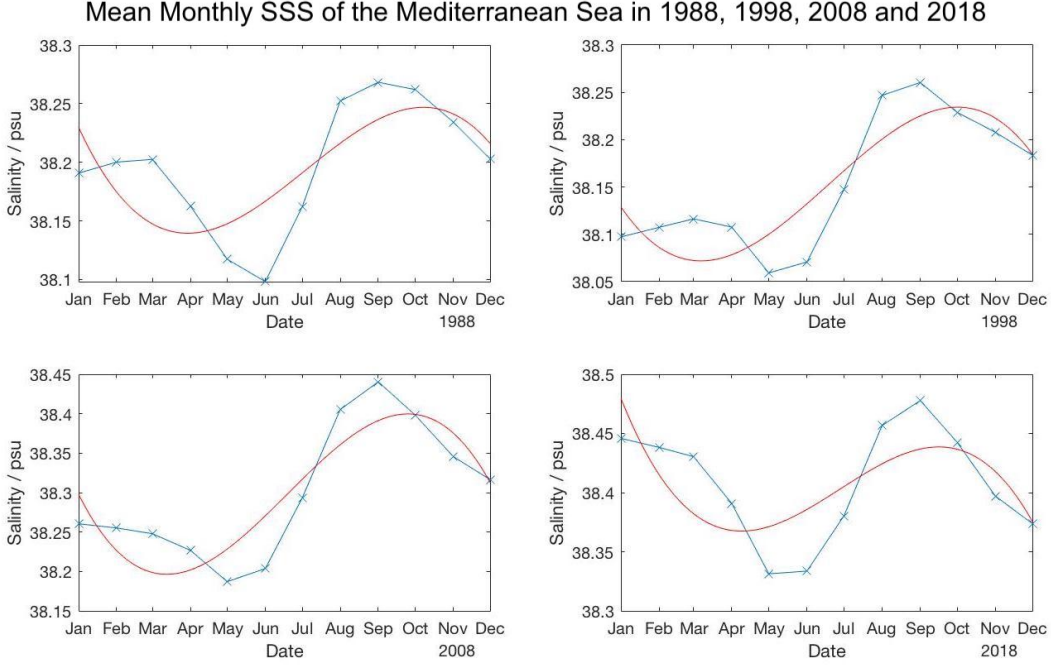


Figure 15: Mean Monthly SSS in the Mediterranean Sea indicates a drop in SSS during spring, with lowest values occurring in May and June. Highest values are typically observed in September.

SSSs present their maximum differences during summer, whilst during winter and autumn the distribution of SSS is more uniform in all regions discussed above.

Results have shown that SSS in each of the above areas increases year-by-year. In order to verify this tendency, results were analysed as with the Mediterranean Sea in Figure 7, and scatter diagrams were produced, with a best-fit straight line indicating the trend for each region.

The gradient of each best-fit straight line was calculated, in order to determine the rate of increase of Annual Mean SSS in each region.

In order to identify extreme values, the green, best-fit curve will be compared to measurements as, in most cases, it allows for larger discrepancies than the straight line would.

The gradient of each best-fit straight line was calculated, in order to determine the rate of increase of Annual Mean SSS in each region.

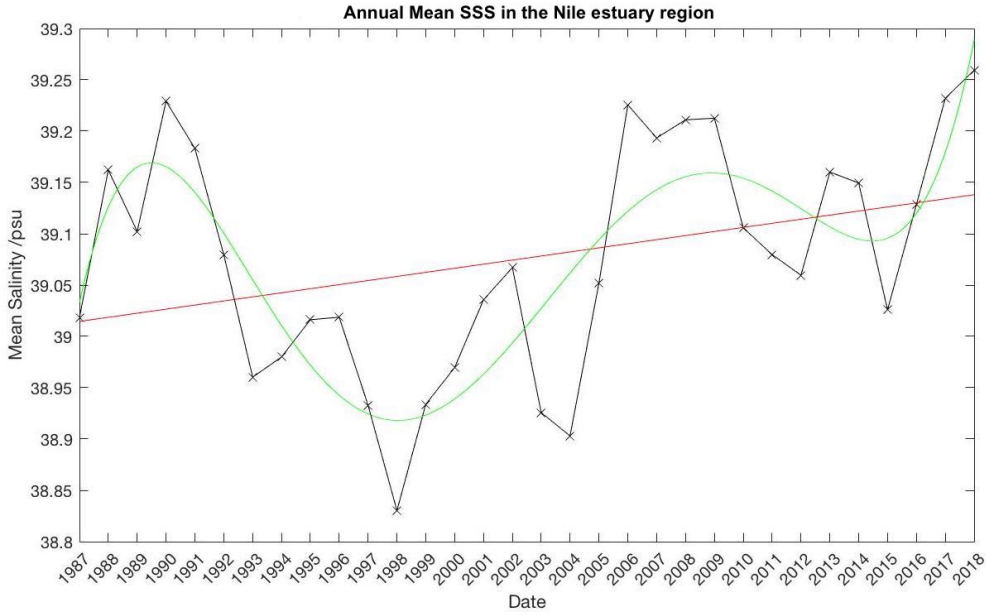


Figure 16: Annual Mean SSS in the Nile estuary region is plotted against time, exhibiting an increasing SSS over the 1987-2018 time period. The green line takes into account fluctuations that have been observed while the red line describes a linearly increasing trend.

The gradient of the line in Figure 16 was calculated to be $0.0040 \text{ psu yr}^{-1}$. Yearly Mean SSS is increasing in the Nile, with an extreme value in 1998, when very low mean SSS was recorded and in 1990 when mean SSS was high.

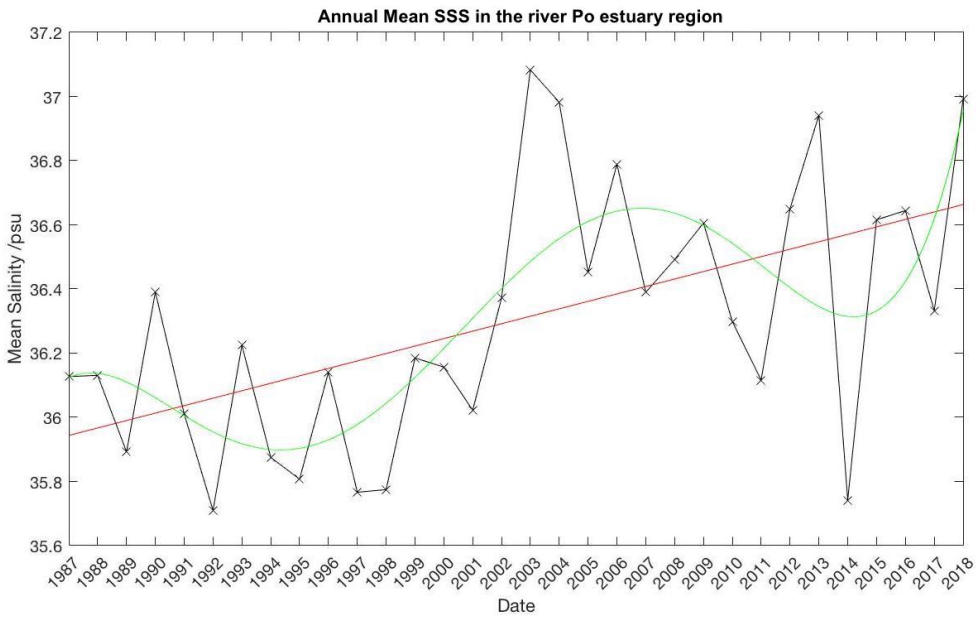


Figure 17: Annual Mean SSS in the Po estuary region is plotted against time, exhibiting a tendency to increase over time. The red line shows a linear increase with time, while the green curve shows a non-linear increase, with a sharp increase in 2018.

Extreme values in Figure 17 include 2003 and 2004 when very Annual Mean SSS was very high, and 2014 when Annual Mean SSS was low. The gradient of the line in Figure 17 was calculated to be $0.0232 \text{ psu yr}^{-1}$.

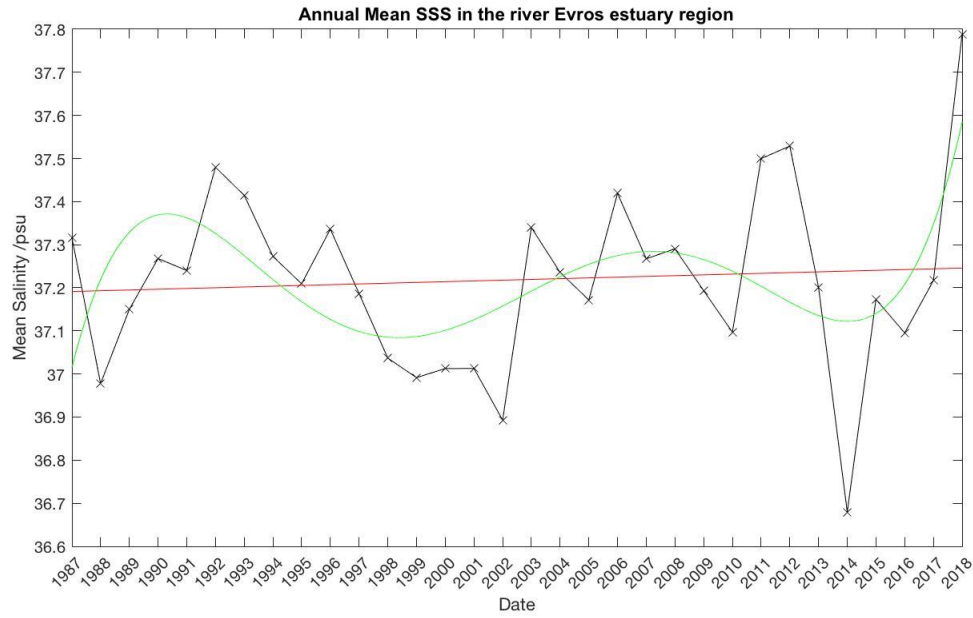


Figure 18: Annual Mean SSS in the Evros estuary region is plotted against time, exhibiting an almost constant SSS over the 1987-2018 time period, though there is an increasing tendency over time. The green line takes into account fluctuations that have been observed while the red line describes a linearly increasing trend.

The gradient of the line in Figure 18 was calculated to be $0.0018 \text{ psu yr}^{-1}$. Extreme values include very low SSS recorded in 2014, while very high SSS in 2018.

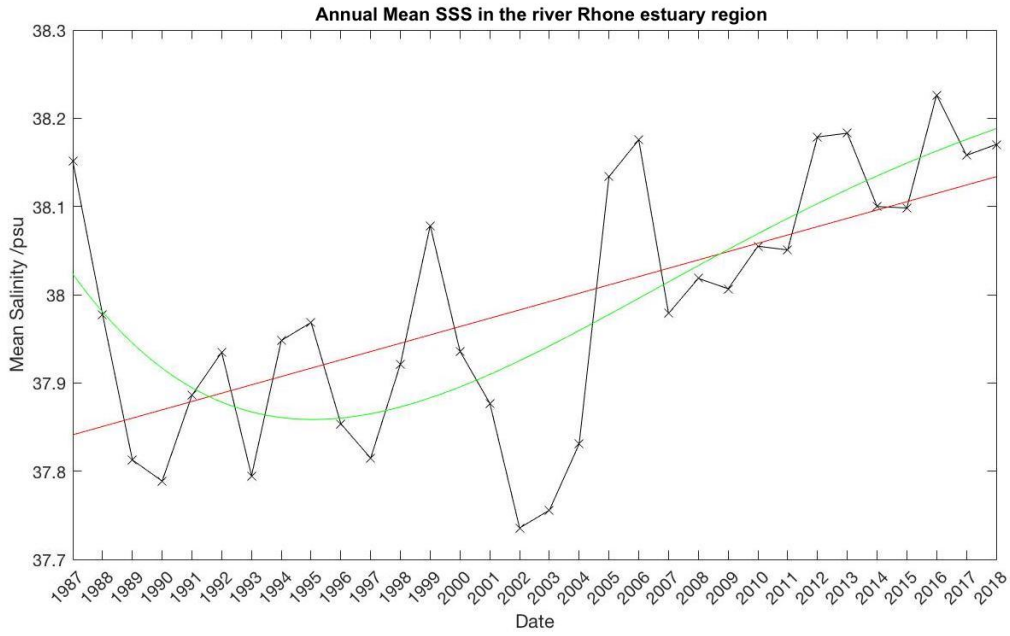


Figure 19: Annual Mean SSS in the Rhone estuary region is plotted against time, exhibiting a tendency to increase over time. In 2002 there was a notable drop in SSS which persisted until 2004, until it escalated again in 2005, when the largest increase in SSS was recorded within this time period. The red line shows the linear increasing trend, while the green line shows a non-linear, increasing trend.

The trend in Figure 19 shows an increase in Annual Mean SSS, and there are several extreme values such as very low Annual Mean SSS in 2002 and 2003 and very high Annual Mean SSS in 1987. The gradient of the line in Figure 15 was calculated to be $0.0094 \text{ psu yr}^{-1}$.

The highest rate of increase in Annual Mean SSS has been determined to be in the region of the Rhone estuary, followed by that of Po, the Nile and Evros.

Figure 20 summarises all above-mentioned observations, more clearly showing that the Nile has the highest Annual Mean SSS values of all regions. Best-fit, fourth-degree polynomial curves are also displayed for comparison.

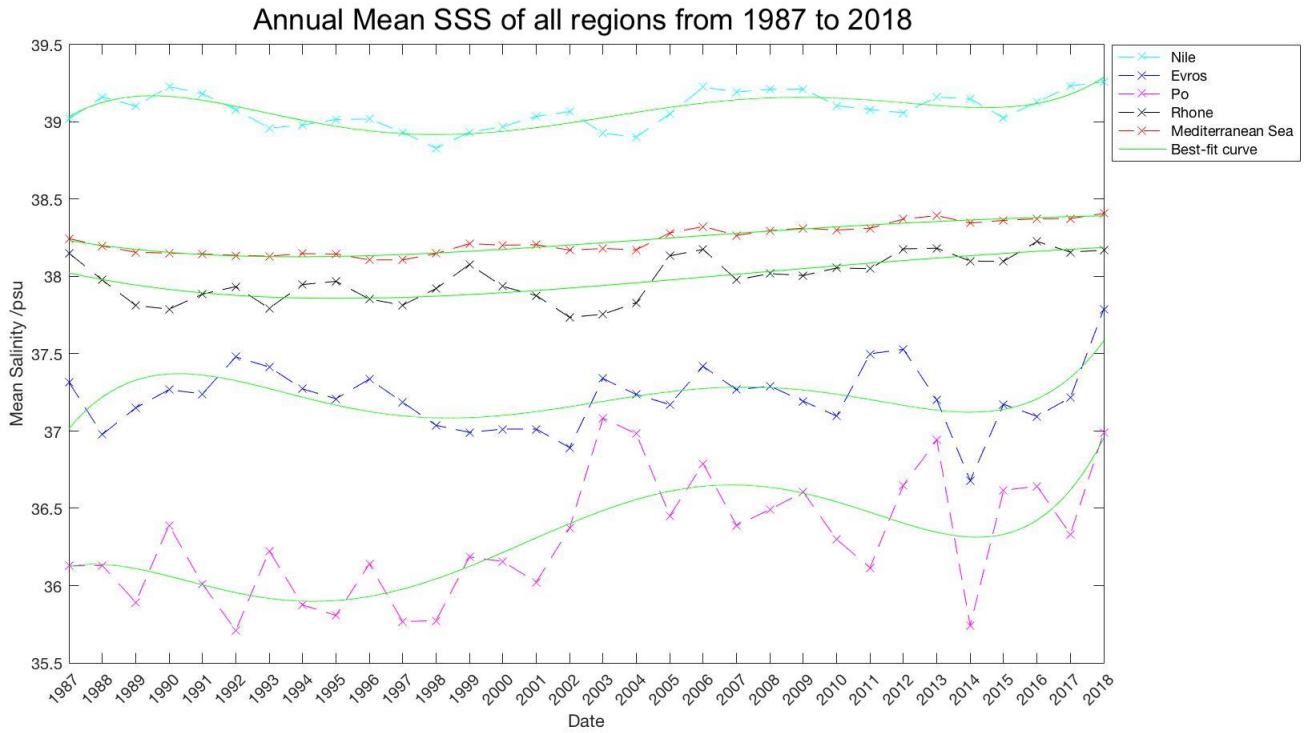


Figure 20: Diagram of SSSs of all regions. While the Po, Rhone, Evros have similar overall SSS values, highest overall SSS was recorded in the Nile estuary region.

An overall increase in Annual Mean SSS persists in all regions over the given time period in either of the two best-fit lines. The Nile has the highest Annual Mean SSS values - around 39 psu -, followed by the Mediterranean Sea as a whole. The Rhone has slightly lower Annual Mean SSS, followed by the Evros. Po has the lowest Annual Mean SSS, with values never exceeding 37.1 psu while other regions' Annual Mean SSS values have never exceeded 38.5 psu and have never been below 37.4 psu.

2.3 Trends in Monthly Mean Sea Surface Temperature (Monthly Mean SST) around river estuaries

For the subsequent analysis of SST for each region, geographical coverage used is listed in Table 1.

The Nile estuary region seems to have Monthly Mean SST values that remain closer to the curve of best-fit as one can observe in Figure 21; a pattern that we have also observed with the region's Monthly Mean SSS. The monthly pattern remains the same, with the peak being in August, and minimum in February and March. It should be noted that overall Monthly Mean SST values are considerably higher than those of other river estuary regions.

Mean Monthly Sea Surface Temperature in the Nile estuary region in 1988, 1998, 2008 and 2018

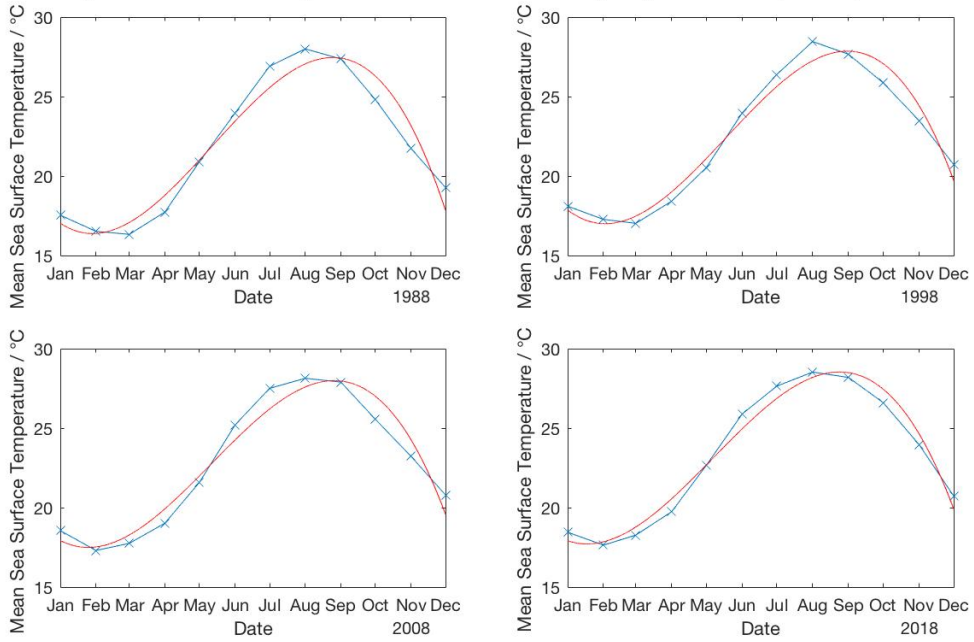


Figure 21: Mean Monthly SST in the Nile' estuary region indicates a drop in SST during autumn, and a rise starting in spring, with lowest values occurring in February and March. Highest values are typically observed in July and August. The data is in close agreement with the red best-fit curve.

There are few differences in the pattern observed in the Evros estuary region (Figure 22) compared to the Rhone and Po; From the graphs of SST of the four years chosen, it is evident that Monthly Mean SST is more likely to peak during July and may as well persist throughout August as well. Minimum Monthly Mean SST is observed during February and March. Minimum Monthly Mean SST reached in the Evros river estuary is higher than those of the Rhone and Po, while maximum Monthly Mean SST is lower than Po, but similar to the Rhone. There seems to have been an increase in Monthly Mean SST from 1988 to 2018, as with above river estuary regions.

Mean Monthly Sea Surface Temperature in the Evros estuary region in 1988, 1998, 2008 and 2018

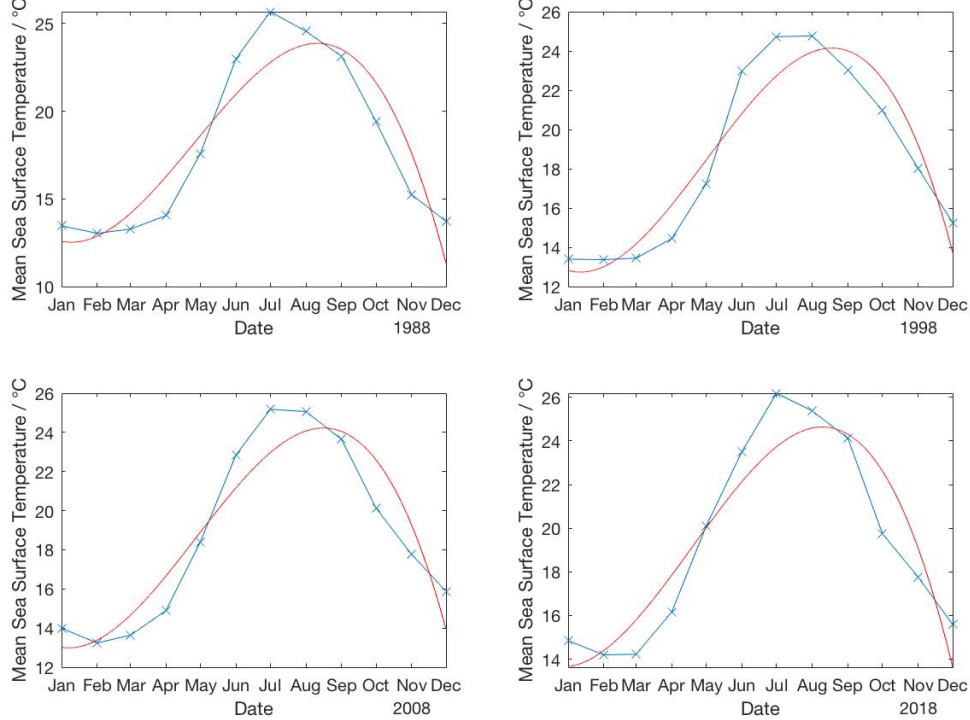


Figure 22: Mean Monthly SST in Evros' estuary region indicates a drop in SST during autumn, and a rise starting in spring, with lowest values occurring in February and March. Highest values are typically observed in July and August.

The trend in the Po estuary region follows a similar pattern as with the Rhone, with temperature increasing after April and falling rapidly after August (Figure 23). Maximum Monthly Mean SST occurs in August and the minimum around February and March. Maximum Monthly Mean SST was lower in 1988 than the following decades and so was the difference between the peak and the minimum point.

Mean Monthly Sea Surface Temperature in the Po estuary region 1988, 1998, 2008 and 2018

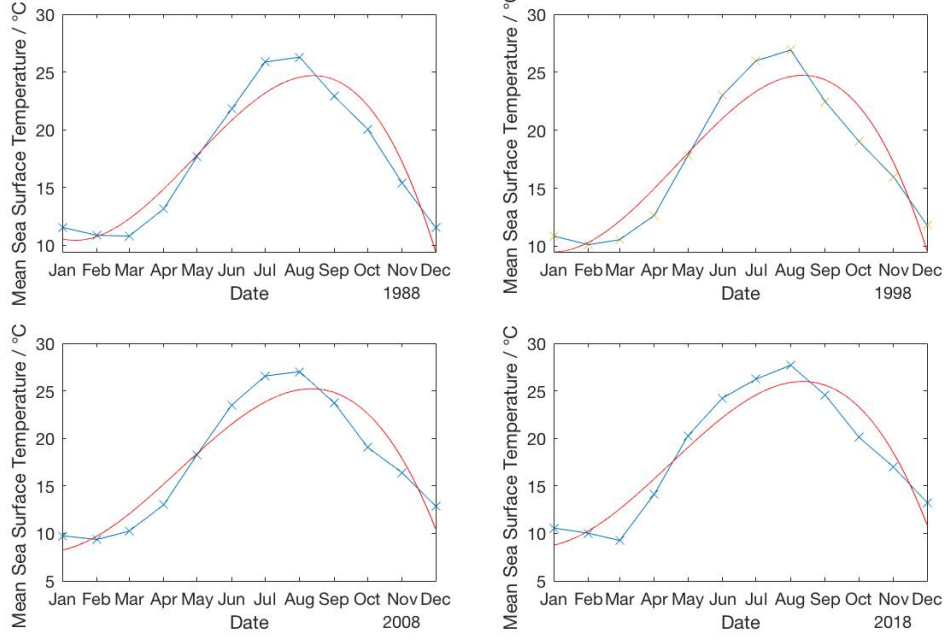


Figure 23: Mean Monthly SST in the Po estuary region indicates a drop in SST during autumn, and a rise in the summer, with lowest values occurring in February and March. Highest values are typically observed in July and August.

In the Rhone estuary region, trend appears in Monthly Mean SST (Figure 24) appears similar between 1988, 1998, 2008 and 2018, with the peak occurring in August and the minimum around February and March. Monthly Mean SST gradually decreases from January until March or February and after April it increases, reaching a maximum in August. It then plummets until December. In 2018, maximum Monthly Mean SST reached in the region rose to 25 °C compared to previous decades when it only reached a maximum of 24 °C. Finally, in 2018 there was a larger difference between minimum and maximum Monthly Mean SST during the year.

Mean Monthly Sea Surface Temperature in the Rhone estuary region 1988, 1998, 2008 and 2018

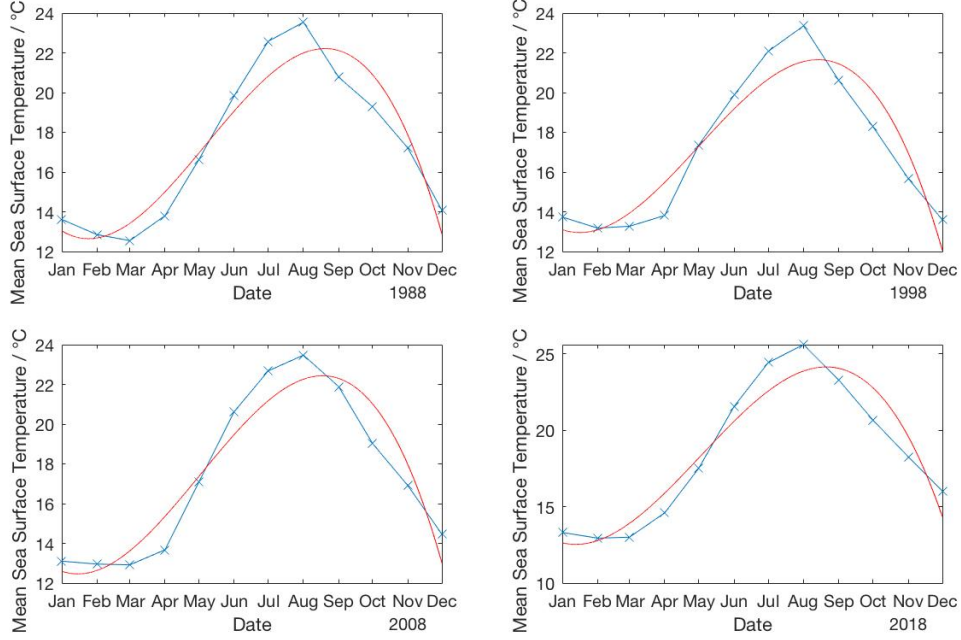


Figure 24: Mean Monthly SST in the Rhone estuary region indicates a drop in SST during autumn, and a rise in the summer, with lowest values occurring in February and March. Highest values are typically observed in July and August.

The tendency of Annual Mean SST (Annual Mean SST) was then investigated in order to verify that it is increasing, as deduced from Figures 21-24. Annual Mean SST was calculated for each year, using Annual Mean SST values and plotting a best-fit straight line.

As was done with SSS, the red best-fit straight line on the graphs, represents a linear increase in Annual Mean SST with time. The green best-fit curve (drawn using the polyval and polyfit functions) depicts a non-linear relationship between Annual Mean SST and time, with fluctuations occurring during certain periods. The gradient of each best-fit straight line was calculated, in order to determine the rate of increase of Annual Mean SST in each region.

Figures 25 - 28 show how Annual Mean SST has changed over the past three decades.

The best-fit straight line in Figure 25 has demonstrated that the Annual Mean SST in the Nile estuary region is increasing by $0.0451 \text{ } ^\circ\text{C yr}^{-1}$.

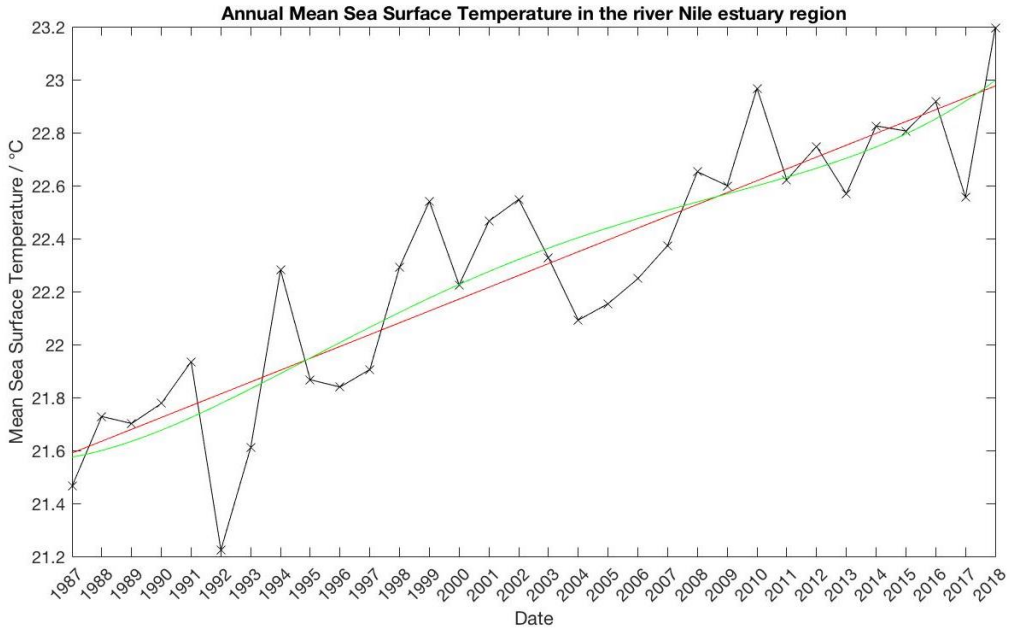


Figure 25: Annual Mean SST in the Nile's estuary region is plotted against time, exhibiting an increasing SST over time. The green line takes into account fluctuations that have been observed while the red line describes a linearly increasing trend.

The trend of the Evros estuary region (Figure 26), there are a few extrema, including higher Annual Mean SST values in 1994, 1999 and 2010. Very low Annual Mean SST values occurred in 2006 and 2017. Calculation of the gradient of the best-fit straight line shows that Annual Mean SST is increasing at a rate of $0.0454 \text{ } ^\circ\text{C yr}^{-1}$.

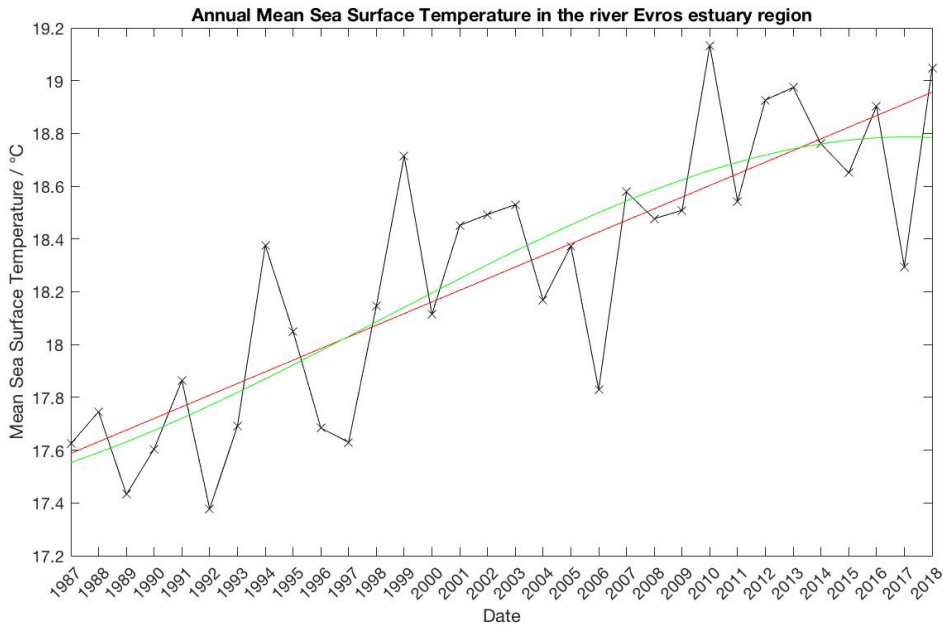


Figure 26: Annual Mean SST in Evros's estuary region is plotted against time, exhibiting an increasing SST over the 1987-2018 time period. The green line takes into account fluctuations that have been observed while the red line describes a linearly increasing trend.

Rate of increase of SST in the Po (Figure 27), is $0.0349 \text{ } ^\circ\text{C yr}^{-1}$.

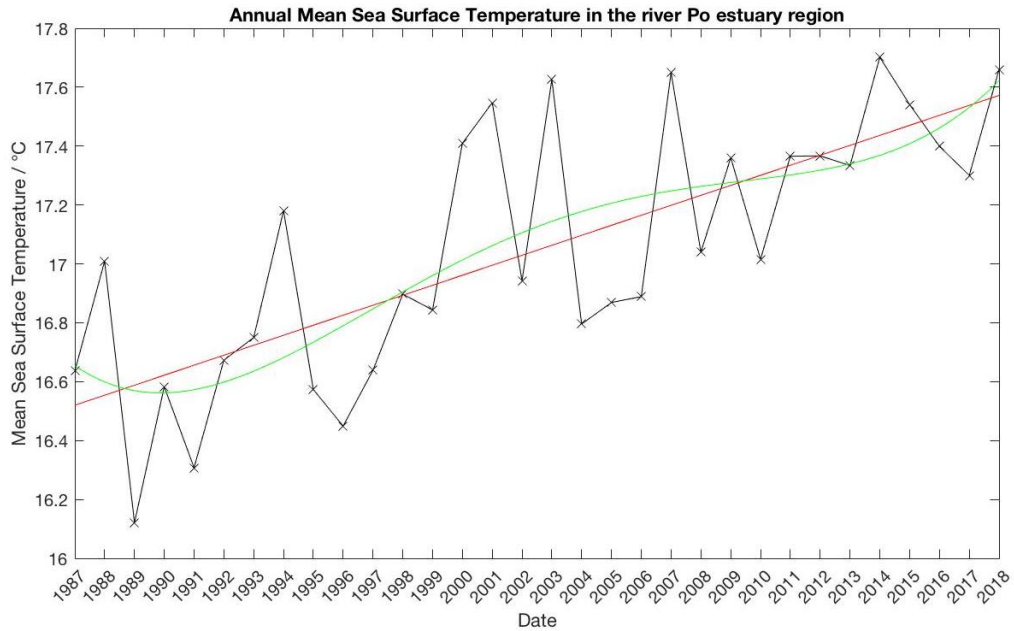


Figure 27: Annual Mean SST in Po's estuary region is plotted against time, exhibiting an increasing SST with time. The green line takes into account fluctuations that have been observed while the red line describes a linearly increasing trend.

In the Rhone (Figure 28), Annual Mean SST has been increasing on average, with an extreme value occurring in 2003. The gradient of the red, best-fit straight line has been calculated to be $0.0229 \text{ } ^\circ\text{C yr}^{-1}$.

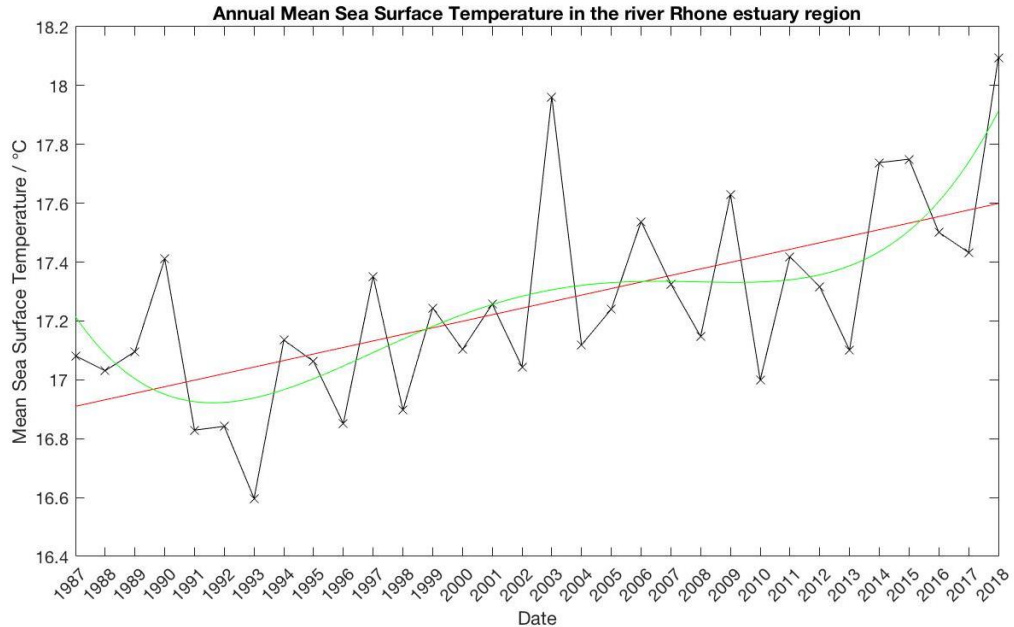


Figure 28: Annual Mean SST in Rhone's estuary region is plotted against time, exhibiting an increasing SST over the 1987-2018 time period. The green line takes into account fluctuations that have been observed while the red line describes a linearly increasing trend.

We therefore conclude that Annual Mean SST is increasing most rapidly in the river Nile estuary region, followed by Evros, the Po and the Rhone.

With the Annual Mean SST in the Mediterranean Sea increasing with $0.0296 \text{ } ^\circ\text{C yr}^{-1}$, a comparison was made between all above-mentioned regions, illustrated in Figure 29. Overall Annual Mean SST values are significantly higher in the Nile, with average value above $21 \text{ } ^\circ\text{C}$, while the Rhone and Po having the lowest Average Annual Mean SSTs, followed by Evros, the Mediterranean Sea as a whole and finally the Nile. Po and the Rhone have average SSTs below $18 \text{ } ^\circ\text{C}$. Evros shows slightly higher SSTs than these rivers, but lower than those of the Mediterranean Sea.

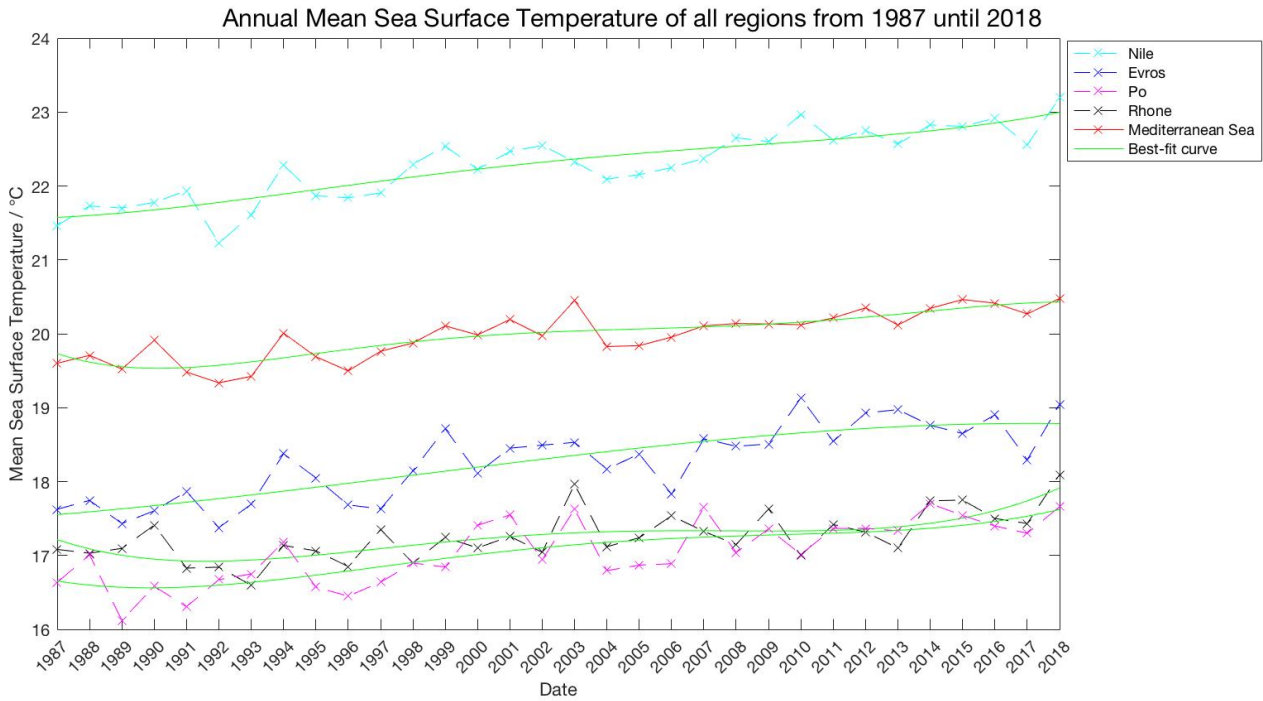


Figure 29: Diagram of SSTs of all regions. Lowest overall SST values were recorded in the Rhone, followed by Po and Rhone which are in close agreement, the Mediterranean Sea as a whole and, lastly, the Nile.

3 Discussion & Conclusions

3.1 Changes in SST

The primary cause of rising SST levels worldwide is climate warming due to excessive amounts of greenhouse gases being released into the atmosphere. Heat from the warming atmosphere raises the temperature of the sea surface. Down-welling currents convey some of this heat to the ocean's deeper layers, which are also warming, though lagging far behind the rise in SST.

Water expands as it warms and the increased volume causes sea level rise. Climate warming is also causing glaciers and continental ice caps to melt, adding water to the ocean and further increasing sea level rise. The rate of global

sea level rise has accelerated over the past few decades.

According to the Intergovernmental Panel on Climate Change (IPCC) in 2013, the warming rate of the upper 75 m of the ocean is 0.11 [0.09 to 0.13]C per decade in the upper 75 m. [2]

Thermal expansion and the increased supply of meltwater from glaciers and continental ice caps could contribute a 1-3m sea level rise by the end of this century (Dasgupta 2007) [3].

Sea surface temperature is projected to continue to increase, depending on the emissions scenario, although more slowly than air temperature over land. In parallel with the rise in sea surface temperature, the frequency and magnitude of marine heatwaves have increased significantly globally and in European seas. This rise is projected to continue rapidly, with increasing impacts on ecosystems and land climate [19].

According to the European Environment Agency, all European seas have warmed considerably since 1870; the warming has been particularly rapid since the late 1970s [19].

In summary, results have shown that SST, SSS and SSH in the Mediterranean Sea, have been increasing, on average, since 1987. This holds for river estuary areas (specifically those of the Nile, Evros, Po and Rhone). Our analysis has shown that SST in the Mediterranean Sea is increasing at a rate of $0.0296 \text{ }^{\circ}\text{C yr}^{-1}$. There has been an overall increase of $0.92 \text{ }^{\circ}\text{C}$ in the upper layer (0-150 m) of the Mediterranean Sea. This is similar to values found by Pastor et al. (2018) of 0.5 C from 1980 to 2000, while Belkin (2009) calculated a higher increase of 1.4 $^{\circ}\text{C}$ from 1978 to 2003 [20].

3.2 Changes in SSS

Our analysis has yielded a rate of increase of $0.088 \text{ psu yr}^{-1}$ in the upper layer of the Mediterranean Sea.

Evaporation of ocean water and formation of sea ice both increase the SSS of the ocean. However these salinity-raising factors are continually counterbalanced by processes that decrease SSS such as the continuous input of freshwater from rivers, precipitation of rain and snow, and melting of ice [25].

Sea evaporation significantly increased since the mid-1970s (0.1–0.2 mm/day/decade) with a tendency toward higher rates of increase during the 1990s. This long-term increase followed a period of evaporation decrease during 1965–75, but overall evaporation has increased since the 1960s by about 10% in total (0.06 mm/day/decade) [21].

Mariotti (2010) studied the relationship between evaporation/precipitation and SST in the Mediterranean finding a significant increase in evaporation since the mid-1970s, preceded by a descent during 1965–1975. In her work, Mariotti states that the evaporation increase was primarily driven by SST increase and remarks the importance of evaporation in observed SSS changes in the Mediterranean [20].

Coupled Model Intercomparison Project Phase 3 (CMIP3) projections for the twenty-first century indicate that the Mediterranean Sea loss of freshwater will accelerate in future decades (Mariotti et al. 2008). Confidence in these projections will depend on our ability to reconcile differences between observations and simulations, better defining past observed changes and improving our understanding and simulation capability [21].

3.3 Changes in SSH

Analysis has shown that SSH in the Mediterranean Sea has been rising by 0.68 mm yr^{-1} .

Sea surface temperature trends are strongly correlated to sea level trends, indicating that at least part of the observed sea level change has a thermal origin [32].

Our results, those of Cazenave et al. (2001) and Tsimplis, Rixen (2002) indicate increases in sea level in the Mediterranean driven by warming of the upper waters. In fact, Cabanes et al. (2001) comparing the global records suggest that after 1993 the temperature changes are the dominant factor globally and no other forcing parameter seems to matter [22].

The Mediterranean Sea in particular, being a semi-enclosed basin, has been experiencing sea level rise differently from the global mean. The estimated trends indicate that Mediterranean mean sea level has been rising at a lower rate than global mean sea level during the second half of the 20th century. The trend for the basin mean sea level over this period is $+0.6 \pm 0.1 \text{ mm yr}^{-1}$; for the period 1961-2000 the Mediterranean trend is $+0.2 \pm 0.1 \text{ mm yr}^{-1}$, much lower than the global mean sea level trend of $+1.6 \pm 0.2 \text{ mm yr}^{-1}$ [33]. Additionally, Tsimplis et al. (2008) found that the average sea level rise in the Eastern Mediterranean is 0.11 m while in the Western Mediterranean is 0.18 m corresponding to mean sea level rise of about 1 mm yr^{-1} and 1.6 mm yr^{-1} respectively over the 21st century [35].

The abovementioned results are similar to the mean sea level rise (SSH rate of increase) of 0.84 mm yr^{-1} for the whole Mediterranean Sea, found for the period 1987-2018 in this paper using data from the Copernicus Marine Service Website. This may indicate that sea level has been, and will continue rising consistently in the future.

3.4 Seasonal Changes of Conditions in Estuary Regions

The Mediterranean summer has occasionally been defined in an extended fashion (e.g. May-September) (Delitala et al., 2000; Sumner et al., 2001), but rainfall re-establishes itself and temperatures start to fall (gradually) in early September as incursive circulation strengthens during October (Wallen, 1970). Many Mediterranean countries, particularly to the west (i.e., southern France, Iberia), experience a sudden peak in precipitation in early October (Barry and Chorley, 1998) that signals the collapse of stable summer conditions. Temperatures drop through October (November in the Aegean), with winter conditions propagating across the majority of the basin (Fig. 2.2), and usually reach a minimum in January, but occasionally in December or February (Lines Escardo, 1977; Furlan, 1977). The majority of the northern basin experiences a secondary rainfall peak in March/April (Trewartha, 1961; Barry and Chorley, 1998) [26].

River discharge is the volume of water flowing through a river channel. This is the total volume of water flowing through a channel at any given point and is measured in cubic metres per second (m^3s^{-1}). The discharge from a drainage basin depends on precipitation, evapotranspiration and storage factors [24]. There is therefore a greater volume of freshwater flowing in river estuaries in the Summer, which as previously mentioned, decreases the SSS of surrounding ocean water in the vicinity. Lower temperatures in winter months result in a lower evaporation rate, also lowering SSS and the opposite occurs during summer months.

One may note that the dominant flood season for the Po River at Pontelagoscuro and Piacenza is Autumn, while the peak discharge volumes are generally observed in late Spring [15]. Variability in Nile discharge is thought to be mainly related to changes in precipitation over the Ethiopian mountains [29]. Annual rainfall over the basin decreases from the south-west (>2000 mm) to the north-east (around 1000 mm), with about 70 per cent occurring between June and September [31]. In the Evros estuary region (Aegean) for instance, the overall spatial SST and SSS distribution pattern is controlled by: distribution of the (colder) Black Sea Waters; advection of the (warmer) Levantine Waters, from the southeastern part of the Aegean; upwelling and downwelling; and, to a lesser extent, but locally important, freshwater riverine inflows [23], which is in agreement with data. Poulos et al. (1997) have found that Mean Monthly SSTs vary from 8 °C in the north during winter, up to 26 °C in the south during summer, which is also in agreement with the data for the Evros estuary region [23]. In the Rhone region, large multi-day rainfall amounts in the winter half-year (October – March) [34]. Results in sections 2.2, and 2.3 for monthly changes of SST and SSS around river estuaries are in agreement with these factors; Higher precipitation and large amounts of snow melting in spring, causes an discharge of a larger volume of freshwater in each estuary region, subsequently causing SSS in the following months to be lowest.

This causes the trends discussed in sections 3.1 and 3.2; higher SSTs in July and August and lowest in February and March, and higher Salinities in spring and autumn and lowest mainly during July.

3.5 Climate Change

The atmospheric concentration of CO₂ has increased during the last century and is expected to double within the next 60 years [Wilson and Mitchell, 1987; Schlesinger and Zhao, 1989].

This increase of the green house gas effect heats the atmosphere and provokes a stronger evaporation at the ocean surface. As water vapor is one of the green house gases, a positive feedback leads to an amplification of the atmospheric warming. Several numerical studies have showed that the air temperature increase of the next century is projected to range from 2 to 7 K and the average precipitation is projected to augment because of the evaporation increase according to trends [27].

Analysis has shown that SSS, SST and SSH have been increasing, in all estuary regions analysed in this report as well as the whole of the Mediterranean Sea. In the twenty-first century, as mean global temperature increases, in the Mediterranean region, precipitation will decrease and temperature will warm 20% more than the global average. Large parts of the Iberian, Balkan, and Anatolian Peninsulas will be affected by a reduction of seasonal precipitation in all seasons [36].

The changing availability of freshwater resources is likely to be one of the most important consequences of projected 21st century climate change for both human and natural systems [30]. Long-term SSS increase has also been connected to a reduction in river discharge (e.g., damming of the Nile River in the 1960s) [21]. Also, since the Rhone is the biggest European river which flows into the Mediterranean Sea, a reduction of its annual discharge could have a significant impact on the sea SSS (as shown for the Nile by Rohling and Bryden [1992] or Bethoux and Gentili [1999]). However, substantial uncertainty remains regarding the precise impacts of climate change on water

resources, in part due to uncertainty in General Circulation Model projections of climate change [30].

Acknowledgements

The author would like to thank Dr. Anastasios Matsikaris for supporting and commenting on this report and the University of Cyprus for facilitating this project. Support of the datasets used is provided by the Copernicus Marine Service Website. The author thankfully acknowledges Bolzon, G., Feudale, L., Solidoro, C., and Crise, A, Cossarini, G., Lazzari, P., Salon, S., Teruzzi, A. and Di Biagio, V. who provided data for this study.

References

- [1] Simoncelli, S., Fratianni, C., Pinardi, N., Grandi, A., Drudi, M., Oddo, P., & Dobricic, S. (2019). Mediterranean Sea Physical Reanalysis (CMEMS MED-Physics) [Data set]. Copernicus Monitoring Environment Marine Service (CMEMS).
[<https://doi.org/10.25423/MEDSEA.REANALYSIS.PHYS.006.004>](https://doi.org/10.25423/MEDSEA.REANALYSIS.PHYS.006.004)
- [2] Rhein, M., S.R. Rintoul, S. Aoki, E. Campos, D. Chambers, R.A. Feely, S. Gulev, G.C. Johnson, S.A. Josey, A. Kostianoy, C. Mauritzen, D. Roemmich, L.D. Talley and F. Wang, 2013: Observations: Ocean. In: *Climate Change 2013: The Physical Science Basis. Contribution of Working Group I to the Fifth Assessment Report of the Intergovernmental Panel on Climate Change* [Stocker, T.F., D. Qin, G.-K. Plattner, M. Tignor, S.K. Allen, J. Boschung, A. Nauels, Y. Xia, V. Bex and P.M. Midgley (eds.)]. Cambridge University Press, Cambridge, United Kingdom and New York, NY, USA.
- [3] Ocean Health Index. (2016). *Sea Surface Temperature* [Online]. Available:
<http://www.oceanhealthindex.org/methodology/components/sea-surface-temperature>
- [4] Ocean Tracks. (2011). *Sea Surface Temperature* [Online]. Available:
<https://oceantacks.org/library/oceanographic-factors/sea-surface-temperature>
- [5] Copernicus Marine Service. *Temperature* [Online]. Available:
<https://marine.copernicus.eu/training/education/ocean-parameters/temperature/>
- [6] C.Fratianni, E.Clementi, S.Simoncelli, "QUality Information Document for Med Physics reanalysis product: MEDSEA.REANALYSIS.PHYS.006.004", 1.5, Sept 2019.
- [7] Knauth L.P. (2011). "Salinity History of the Earth's Ocean". In: Reitner J., Thiel V. (eds) Encyclopedia of Geobiology. Encyclopedia of Earth Sciences Series. Springer, Dordrecht.
https://doi.org/10.1007/978-1-4020-9212-1_177
- [8] Copernicus Marine Service. *Sea Level* [Online]. Available:
<https://marine.copernicus.eu/training/education/ocean-parameters/sea-level/>
- [9] N.R. Peacock and S.W. Laxon, "Sea surface height determination in the Arctic Ocean from ERS altimetry," *Journal of Geophysical Research*, vol. 109, C07001, pp. 2, doi:10.1029/2001JC001026, Jul 2004 .

- [10] M. Salah. (2019, Aug. 30). *Mediterranean Sea* [Online]. Available:
<https://www.britannica.com/place/Mediterranean-Sea>
- [11] M.J. Booij, D. Tollenaar, E. van Beek, J.C.J. Kwadijk, "Simulating impacts of climate change on river discharges in the Nile basin," *Physics and Chemistry of the Earth*, Parts A/B/C, vol. 36, 13, pp. 696-709, ISSN 1474-7065, 2011.
<https://doi.org/10.1016/j.pce.2011.07.042>.
- [12] M.M. El-Kammash et al. "Nile River" in *Encyclopædia Britannica*. Encyclopædia Britannica, inc., 2019 [Online]. Available:
<https://www.britannica.com/place/Nile-River>
- [13] BiodiversityEast. *The Evros River* [Online]. Available:
<https://www.bio-e.org/lib/evros-river>
- [14] P. Veyret and A. Diem. "Nile River" in *Encyclopædia Britannica*. Encyclopædia Britannica, inc., 2019 [Online]. Available:
<https://www.britannica.com/place/Nile-River>
- [15] A. Montanari, "Hydrology of the Po River: looking for changing patterns in river discharge," *Hydrol. Earth Syst. Sci. Discuss.*, 9, 6689–6713, 2012.
www.hydrol-earth-syst-sci-discuss.net/9/6689/2012/ doi:10.5194/hessd-9-6689-2012
- [16] The Editors of Encyclopaedia Britannica. "Po River" in *Encyclopædia Britannica*. Encyclopædia Britannica, inc., 2019 [Online]. Available:
<https://www.britannica.com/place/Po-River>
- [17] Lagerloef G. (2014) *Sea Surface Salinity*. In: Njoku E.G. (eds) Encyclopedia of Remote Sensing. Encyclopedia of Earth Sciences Series. Springer, New York, NY. https://doi.org/10.1007/978-0-387-36699-9_165
- [18] R.H. Stewart. *Introduction To Physical Oceanography*, 2008 ed. June 3, 2009, pp. 73-75.
- [19] European Environment Energy. *Sea surface temperature* [Online]. Available:
<https://www.eea.europa.eu/data-and-maps/indicators/sea-surface-temperature-3/assessment>
- [20] F. Pastor, J.A. Valiente, & J.L. Palau. "Sea Surface Temperature in the Mediterranean: Trends and Spatial Patterns (1982–2016)," *Pure Appl. Geophys.*, 175, pp. 4017–4029,
doi:10.1007/s00024-017-1739-z, 2018. 2
- [21] A. Mariotti, "Recent Changes in the Mediterranean Water Cycle: A Pathway toward Long-Term Regional Hydroclimatic Change?," ESSIC, Univ. of Maryland, College Park, College Park, Maryland, and ENEA, Rome, Italy, March 2010.
- [22] M. N. Tsimplis, and M. Rixen, "Sea level in the Mediterranean Sea: The contribution of temperature and salinity changes," *Geophys. Res. Lett.*, 29(23), 2136,
doi:10.1029/2002GL015870, 2002.

- [23] S.E. Poulos, P.G. Drakopoulos, M.B. Collins, "Seasonal variability in sea surface oceanographic conditions in the Aegean Sea (Eastern Mediterranean): an overview," *Journal of Marine Systems*, vol. 13, 1–4, pp. 225-244, ISSN 0924-7963, doi:10.1016/S0924-7963(96)00113-3, 1997.
- [24] Internetgeography. *discharge* [Online]. Available:
<http://www.geography.learnontheinternet.co.uk/topics/discharge.html>
- [25] Nasa Science. *Salinity* [Online]. Available:
<https://science.nasa.gov/earth-science/oceanography/physical-ocean/salinity>
- [26] A. E. Harding, "The Mediterranean environment" in *Changes in Mediterranean Climate Extremes: Patterns, Causes, and Impacts of Change*, Ph.D. dissertation, Cim. Res. Un., UEA, Norwich, 2006.
- [27] Etchevers, P., Golaz, C., Habets, F., and Noilhan, J., "Impact of a climate change on the Rhone river catchment hydrology," *J. Geophys. Res.*, 107(D16), doi:10.1029/2001JD000490, 2002.
- [28] ESA. *Exercise 2: Sea surface height* [Online]. Available:
https://www.esa.int/SPECIALS/Eduspace_Weather_EN/SEM7D0L1YHH_0.html#:~:text=The%20sea%20surface%20can%20then,is%20higher%20than%20the%20geoid
- [29] Riehl, H., M. El-Bakry, and J. Meitín, "1979: Nile River Discharge," *Mon. Wea. Rev.*, 107, 1546–1553, 1979.
[https://doi.org/10.1175/1520-0493\(1979\)107;1546:NRD;2.0.CO;2](https://doi.org/10.1175/1520-0493(1979)107;1546:NRD;2.0.CO;2).
- [30] Kingston, D. G. and Taylor, R. G., "Sources of uncertainty in climate change impacts on river discharge and groundwater in a headwater catchment of the Upper Nile Basin, Uganda, Hydrol." *Earth Syst. Sci.*, 14, 1297–1308, 2010. <https://doi.org/10.5194/hess-14-1297-2010>.
- [31] Conway, D. (2000), "The Climate and Hydrology of the Upper Blue Nile River," *Geographical Journal*, 166, pp. 49–62. doi:10.1111/j.1475-4959.2000.tb00006.x
- [32] A. Cazenave, C. Cabanes, K. Dominh, S. Mangiarotti, "Recent sea level change in the Mediterranean Sea revealed by Topex/Poseidon satellite altimetry," *Geophys. Res. Lett.*, vol. 28, 8, pp. 1607-1610, Apr 2001.
- [33] European Science Foundation. D. Gomis, M. Tsimplis, M. Marcos, L. Fenoglio-Marc, B. Pérez, F. Raicich, I. Vilibić, G. Wöppelmann, S. Monserrat, G. Jordà, "MedCLIVAR – Mediterranean CLImate VARiability: Sea Level Rise and its Forcing in the Mediterranean Sea" [Online], Available:
https://digital.csic.es/bitstream/10261/93349/1/C4_GOMIS_TH242A.pdf
- [34] Wit, M.J.M., de and Buishand, T.A., 2007. Generator of Rainfall And Discharge Extremes (GRADE) for the Rhone and Meuse basins. Rijkswaterstaat RIZA report 2007.027/KNMI publication 218. Lelystad, The Netherlands.
- [35] M.N. Tsimplis, M. Marcos, S. Somot, "21st century Mediterranean sea level rise: Steric and atmospheric pressure contributions from a regional model," *Global and Planetary Change*, vol. 63, 2–3, pp. 105-111, ISSN 0921-8181, 2008.

- [36] Lionello, P., Scarascia, L. "The relation between climate change in the Mediterranean region and global warming," *Reg Environ Change*, vol. 18, 1481–1493 (2018).
<https://doi.org/10.1007/s10113-018-1290-1>